Bioinspired Self-Healing Vitrimer from Epoxidised Palm Oil Reinforced with Nanofibrillated Cellulose and Activated Carbon

Chuan Li Lee [a,b] Balkis Fatomer A. Bakar,[a,c,*] Kit Ling Chin [a,*] Luqman Chuah Abdullah [b,d] Xian Foong Lee,[c] and Qi Yong Wong [c]

** Corresponding authors: bfatomer@upm.edu.my; c_kitling@upm.edu.my*

DOI: 10.15376/biores.21.2.4457-4489

GRAPHICAL ABSTRACT

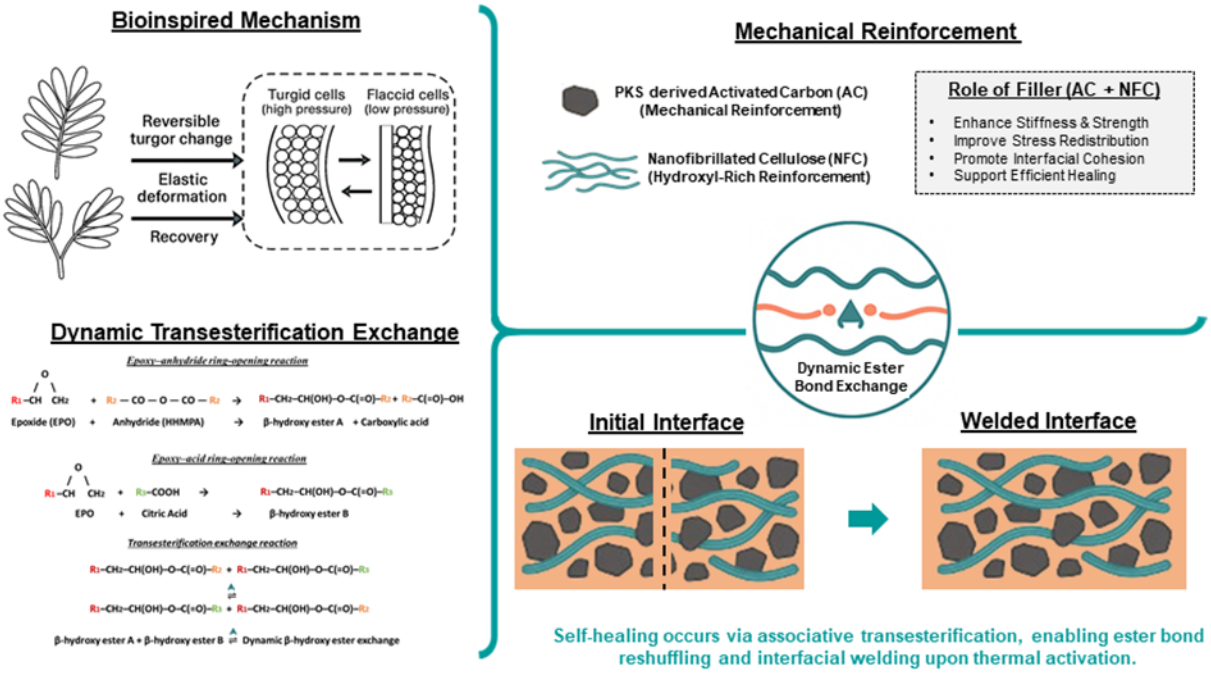

Bioinspired Self-Healing Vitrimer from Epoxidised Palm Oil Reinforced with Nanofibrillated Cellulose and Activated Carbon

Chuan Li Lee [a,b] Balkis Fatomer A. Bakar,[a,c,*] Kit Ling Chin [a,*] Luqman Chuah Abdullah [b,d] Xian Foong Lee,[c] and Qi Yong Wong [c]

A vitrimer composite based on epoxidised palm oil (EPO) was reinforced with nanofibrillated cellulose (NFC) and palm kernel shell (PKS)-derived activated carbon as complementary bio-based fillers. The loadings of NFC and activated carbon were varied to examine their influence on the thermal, mechanical, chemical, and healing-reprocessing behaviour of the EPO vitrimer network. The synergistic interaction between these fillers preserves dynamic bond exchange within the vitrimer network, enabling effective thermal welding in which the welded interface becomes seamless after treatment. This dynamic network behaviour was further reflected in dynamic mechanical and creep-recovery analyses, which revealed the influence of filler content on network mobility. A higher filler content (5 wt% of each filler) enhanced stiffness but restricted network rearrangement, leading to incomplete strain recovery. In contrast, the composite containing 4 wt% of each filler achieved complete strain recovery (100%) while exhibiting strong viscoelastic damping behaviour (tan δ ~ 1.36), indicating efficient molecular relaxation during the glass-transition process. FESEM showed improved interfacial continuity within the synergistic system, where NFC extends between activated carbon particles and the vitrimer matrix to maintain local network integrity and facilitate stress transfer. The rigid carbon phase also limits solvent diffusion within the matrix, contributing to improved solvent resistance of the vitrimer composite.

DOI: 10.15376/biores.21.2.4457-4489

Keywords: EPO vitrimer; Dynamic covalent network; Activated carbon; NFC; Self-healing behaviour

*Contact information: a: Institute of Tropical Forestry and Forest Products, Universiti Putra Malaysia, 43400 UPM Serdang, Selangor, Malaysia; b: Faculty of Biotechnology and Biomolecular Sciences, Universiti Putra Malaysia, Serdang 43400, Selangor, Malaysia; c: Faculty of Forestry and Environment, Universiti Putra Malaysia, Serdang 43400, Selangor, Malaysia; d: Department of Chemical and Environmental Engineering, Faculty of Engineering, Universiti Putra Malaysia, Serdang 43400, Selangor, Malaysia; *Corresponding authors: bfatomer@upm.edu.my; c_kitling@upm.edu.my*

INTRODUCTION

Plastics have become globally dominant because they combine high mechanical strength, low density, excellent processability, and low production cost. This combination of performance and affordability has driven global production from only a few million tonnes in the 1950s to more than 400 million tonnes per year, a trend that continues alongside rising carbon emissions and global temperatures (Kelly *et al.* 2025). However, the inherent properties that make plastics convenient to produce also cause their persistence in the environment. Most plastic waste originates from short-lived consumer products that

degrade very slowly, accumulating in landfills, rivers, oceans, and terrestrial ecosystems, with long-term ecological and climatic consequences (Akash *et al.* 2025). Malaysia faces a comparable challenge, with national assessments indicating that post-consumer plastic waste exceeds 1.07 million tonnes per year (de Jong *et al.* 2025). Although plastics are technically recyclable, an estimated 81% of their material value is lost due to inefficient recovery and recycling systems, resulting in approximately USD 1.1 billion in lost economic value annually (WWF 2022). If global production continues to grow at around three and a half percent per year, plastics alone could emit nearly three gigatonnes of carbon dioxide annually by 2050, even under scenarios of significant energy sector decarbonisation (de Jong *et al.* 2025). This projection highlights the urgent need to reduce reliance on fossil-based polymer feedstocks and to develop sustainable polymer composites that combine high structural performance with recyclability, reparability and circular life-cycle management.

The escalating accumulation of plastic waste worldwide has intensified the search for sustainable materials capable of repairing themselves, adapting to external stimuli, and extending service lifetimes, thereby reducing disposal rates and minimizing environmental burden. Natural systems offer strong inspiration for such materials, as many biological structures possess intrinsic self-healing and adaptive capabilities that maintain functionality under changing conditions. The thigmonastic movement of *Mimosa pudica* provides a well-known example of rapid yet reversible deformation: mechanical stimulation redistributes turgor pressure within the pulvinus, driving leaflet closure through the elastic reorientation of cellulose microfibrils in the cell wall. Because the deformation remains within the elastic domain, the leaflet fully recovers its original structure once turgor pressure is restored, without requiring physiological reconstruction (Lou *et al.* 2025; Nakata and Takahara 2022). Inspired by such mechanisms, biomimetic materials aim to capture functional principles such as self-repair, structural adaptability, and stimulus-responsive behaviour (Wang *et al.* 2023). In this context, vitrimers provide a suitable polymer platform, as their permanently cross-linked networks can undergo dynamic covalent exchange, allowing reshaping, welding, and recovery under thermal stimulus while maintaining structural integrity (Lee *et al.* 2025b).

Previous work has demonstrated that vitrimeric behaviour can be successfully achieved using a traditional petrochemical epoxy matrix (Lee *et al.* 2025a). However, reliance on a petroleum-based epoxy backbone raises significant concerns regarding long-term sustainability, environmental impact, and potential toxicity, reflecting the broader limitations of fossil-derived polymers in achieving circular and environmentally responsible materials (Álvarez *et al.* 2025). To address these challenges, the present work focuses on epoxidised vegetable oils (EVO) as bio-derived alternatives to fossil-based epoxies. EVO offer several inherent advantages: they are sourced from renewable biomass, exhibit low toxicity, possess biodegradable aliphatic structures, and are highly compatible with dynamic covalent chemistries due to their epoxy bearing triglyceride architecture (Maisonneuve *et al.* 2013; Ribeiro *et al*. 2025; Yan *et al.* 2022). In particular, epoxidised palm oil (EPO) is well suited to Malaysia's resource landscape. Malaysia's oil palm sector generates more than 100 million tonnes of dry biomass each year, including trunks, fronds, empty fruit bunches, and palm kernel shells (Anonymous 2025). All of these biomass materials remain largely underutilised despite their potential for value added applications. In parallel, the industry produces substantial quantities of palm oil that can be epoxidised into EPO, a renewable and chemically adaptable precursor. This steady and locally available resource base makes EPO a practical and sustainable alternative to petrochemical

epoxy monomers for developing advanced polymer composites.

Unlike conventional vitrimer composites that rely on long-chain polymeric backbones to achieve entanglement-driven stiffness and high glass transition temperatures, EPO consist of short, triglyceride-based molecular architectures (Ogori 2020; Stavila *et al.* 2023). Prior studies have shown that epoxy networks derived from EPO generally exhibit lower glass transition temperatures and storage moduli than petroleum-based epoxy resins, which can be attributed in part to their relatively low epoxy functionality and the resulting reduced crosslink density (Mauro *et al.* 2020). Nevertheless, recent reports suggest that vitrimer-like behaviour is not strictly dependent on long polymeric backbones, as heating above T_g produces elastomeric behaviour while exchange reactions remain too slow to rearrange network topology (Fang *et al.* 2020; Javier and Toro 2021). On this basis, the present work raises the question of whether vitrimer like dynamic network behaviour and self-healing functionality can emerge in a highly crosslinked, short-backbone EPO system.

Bio-based epoxy resins such as EVO typically exhibit lower mechanical properties, including reduced stiffness, strength, and toughness, compared with conventional epoxy composites (Álvarez *et al.* 2025; Kumar *et al*. 2020; Zhang *et al.* 2023). To address these limitations, mechanical reinforcement through the incorporation of suitable fillers is required to improve stiffness, interfacial integrity, and structural recovery in biocomposite networks. In the authors' previous work, palm kernel shell (PKS)-derived activated carbon was shown to function as an effective thermal-mechanical reinforcement in epoxy-based vitrimer composites, enhancing stiffness, stabilising deformation, and promoting more uniform heat distribution during network rearrangement. However, activated carbon contributes limited catalytic activity and cannot independently regulate nanoscale mobility within the vitrimer structure (Lee *et al.* 2025a).

To complement this limitation, nanofibrillated cellulose (NFC, which also is called CNF) was incorporated to reinforce the vitrimer composite. NFC has been reported as promising reinforcement agents in polymer nanocomposites owing to their renewable origin and nanoscale fibrillar structure, which contribute to improved structural integrity in polymer matrices (Alwan *et al.* 2024). Additionally, the synergistic interaction between NFC and activated carbon in shaping the properties of EPO-based vitrimers remains insufficiently explored particularly regarding how NFC-assisted interactions may strengthen the functional role of activated carbon and how this cooperation contributes to the material's self-healing behaviour. A clearer understanding of this interaction would help guide the future development of fully bio-derived vitrimer materials.

A meaningful research gap remains in understanding the synergistic interactions between NFC, activated carbon, and bio-derived EPO vitrimer networks. Addressing this gap is important for developing renewable vitrimer composites that balance stiffness, molecular mobility, reprocessability, and environmental sustainability. This study develops a bioinspired self-healing vitrimer composite based on EPO, incorporating NFC and PKS-derived activated carbon as reinforcing fillers. By systematically varying the loadings of both fillers, this work provides a foundational and exploratory assessment of their influence on thermal, mechanical, chemical, and reprocessing-healing behaviour. The study therefore provides mechanistic insight into how the integrated effects of these fillers influence the structural and dynamic behaviour of EPO-based vitrimer networks, while highlighting the potential of Malaysia's oil palm biomass as a feedstock for value-added, sustainable polymer composites within a circular economy framework.

EXPERIMENTAL

PKS-derived Activated Carbon *via* Chemical and Physical Activation

Palm kernel shell derived activated carbon was prepared according to the method described in our previous study (Lee *et al.* 2025a), using biomass milled to an average particle size of approximately 85 µm.

Preparation of EPO-Based Vitrimer Composite

Epoxidised palm oil (EPO), supplied by MPOB (oxirane oxygen 3.2 %; acid value 0.7 mg KOH/g), served as the precursor matrix. The EPO was mixed with hexahydro-4-methylphthalic anhydride (HHMPA) at a stoichiometric ratio of 1:3 and stirred for 15 min to achieve a uniform matrix blend. Nanofibrillated cellulose (NFC) was incorporated at loadings of 3, 4, and 5 wt.%, followed by mechanical stirring at 600 rpm for 15 min to promote adequate dispersion. Citric acid (3 wt.%) was introduced to facilitate the curing process, and the formulation was subsequently mixed for an additional 10 min to enhance uniformity. Pre-dried PKS-derived activated carbon was then added at 3, 4, and 5 wt.% and blended for a further 10 min to ensure homogeneous distribution of the microscale filler. A vitrimer composite containing 4 wt.% activated carbon without NFC was prepared as the control for comparative evaluation. The prepared mixtures were transferred to a humidity-controlled chamber for pre-curing at 90 °C for 24 h. Final curing was then carried out in an oven at 140 °C for an additional 72 h to complete network formation. Following curing, all vitrimer composites were placed in a conditioning room to stabilise temperature and humidity prior to thermal, mechanical, and spectroscopic evaluation.

Characterization and Evaluation

Comprehensive characterization was conducted to examine both the mechanical behaviour and the self-healing capability of the vitrimer composites. The evaluation of self-healing (thermal welding) performance employed a combination of mechanical and microscopic techniques. Following the procedure adapted from Chong *et al*. (2021), vitrimer composite specimens were cut to a size of 2 mm × 5 mm × 40 mm, as depicted in the dimensional overview in Figure 1(a). Two specimens were then positioned in an overlapping configuration and thermally activated at 140 °C for 3 h while applying a compressive load corresponding to 10% deformation to promote interfacial welding. After heating, the interface formed between the two overlapping samples was examined under an optical microscope to evaluate interfacial rejoining. Qualitative observation of surface recovery was further performed using a Nikon SMZ1270 stereo/photomicroscope to determine the extent of morphological restoration along the welded region. Subsequently, field emission scanning electron microscopy (FESEM) was employed to characterise the microstructural features at the welding line and to confirm interfacial bonding, using a Tescan Clara 2023 instrument.

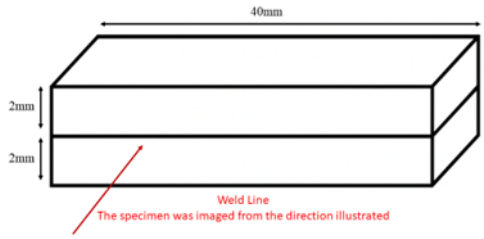

Fig. 1(a). Dimensions and structural arrangement of the test specimens for the self-healing evaluation

In addition to self-healing studies, a suite of chemical, thermal and mechanical analyses was performed to elucidate structural interactions and property evolution within the composites. Fourier Transform Infrared Spectroscopy (FTIR, PerkinElmer Spectrum 100 IR, Tokyo, Japan) was used to identify functional groups and bond rearrangements, while Thermogravimetric Analysis (TGA, PerkinElmer TGA 8000, USA) provided insight into thermal degradation pathways and residue formation. Creep measurements were performed in tensile film mode using a tension film clamp, following a modified procedure adapted from (Xia *et al.* 2024). Both pristine and reprocessed vitrimer materials were tested to evaluate the effect of reprocessing on creep-recovery behaviour. The material processing and reprocessing procedure is illustrated in Figure 1(b). The vitrimer composite was fragmented into smaller pieces and subsequently compression moulded at 180 °C for 15 min to produce a homogeneous film. The creep testing setup is presented in Figure 1(c). A constant load of 20 g was applied, and strain was continuously recorded during the creep stage (1-5 min), followed by the recovery stage (5-10 min) after load removal. The strain, ε(t), was calculated using Eq. 1,

$$\varepsilon(t) = \Delta L(t)/L_0 \quad (1)$$

where $\Delta L(t)$ is the change in length at time t, and the creep-recovery behaviour was evaluated based on the time-dependent strain response.

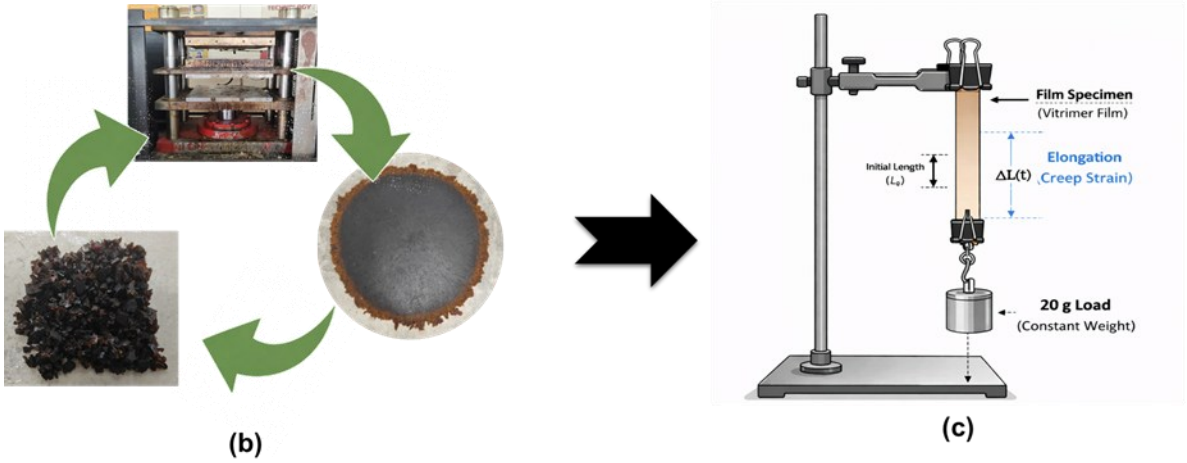

Fig. 1. (b) Reprocessing of vitrimer composites; **(c)** Schematic of creep-recovery test

Dynamic Mechanical Analysis (DMA, TA Instruments Q800 DMA/SDTA e, New Castle, DE, USA) was subsequently employed to determine viscoelastic parameters, including the storage modulus and tan δ (damping factor), which were used to identify the glass-transition region. DMA was also used to examine the viscoelastic response of both pristine and reprocessed vitrimer samples. These analyses enabled a detailed evaluation of the vitrimer network's thermal stability and temperature-dependent mechanical behaviour. The solvent resistance of the vitrimer composites also was evaluated by immersing the samples in different solvents, including water, toluene, methanol, 1,4-dioxane, ethyl acetate, chloroform, and acetone, at room temperature for 24 h. The swelling ratio and gel content were calculated to assess the solvent stability of the vitrimer network (Lee *et al.* 2025a).

RESULTS AND DISCUSSION

Effect of Activated Carbon and NFC Loading on Thermal Welding of the Vitrimer Composites

A class of thermoplastic like thermosets termed vitrimers has been developed with extensive applications, in which welding plays a central and fundamental role, effectively functioning as a form of self-healing through dynamic covalent bond exchange (Shi *et al.* 2023). Figure 2 presents the influence of activated carbon and NFC loading on the thermal welding behaviour of EPO-based vitrimer composites, which proceeds through interfacial welding, revealing how variations in filler loading modulate network reconfiguration during thermal activation. A vitrimer with 4 wt.% activated carbon without NFC was used as the control. It exhibited a visible interface after thermal treatment, indicating limited interfacial reconnection. Rigid particulate fillers such as carbon particles tend to restrict polymer chain mobility at the filler-matrix interface, leading to hindered chain interdiffusion and reduced interfacial entanglements, which in turn limit interface healing and weld strength in polymer nanocomposites (Bonardd *et al*. 2023).

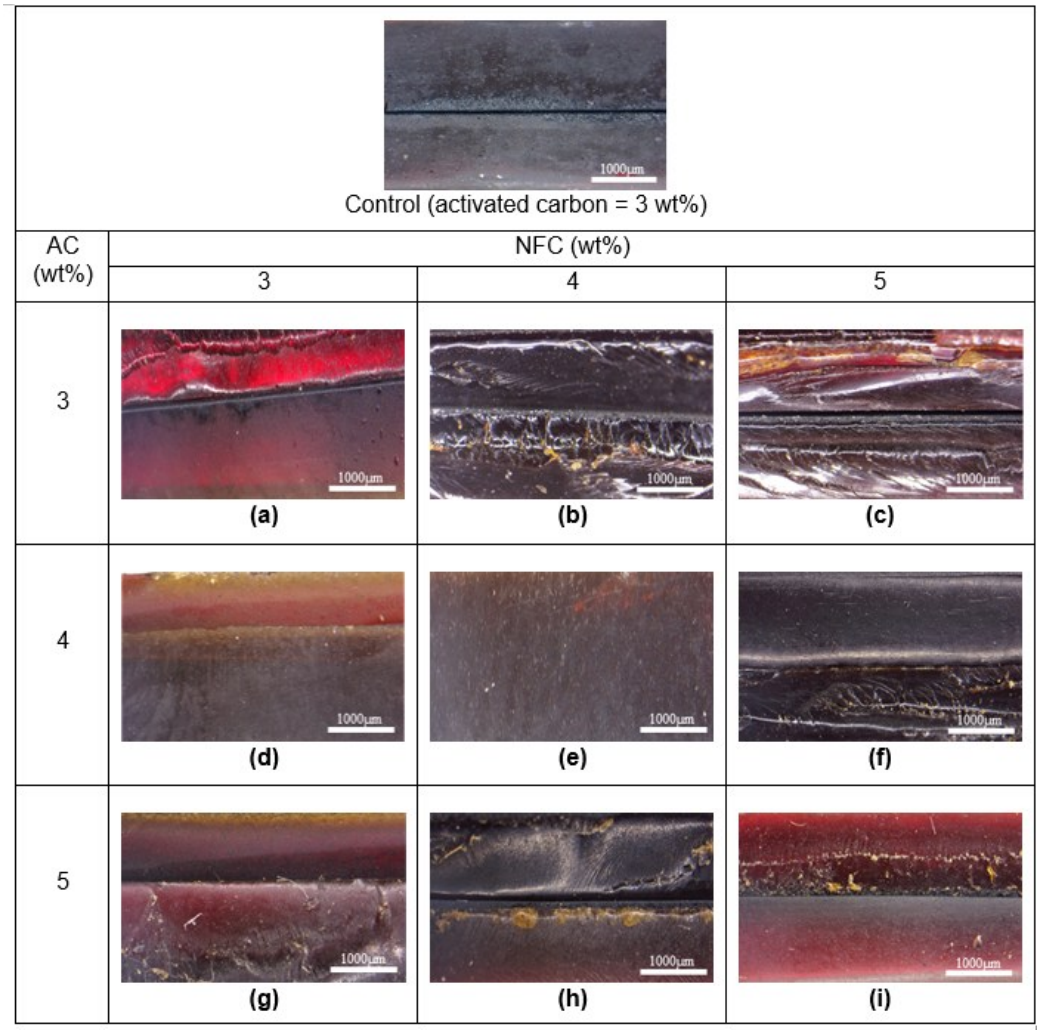

Fig. 2. Surface morphology of welded vitrimer composites for the 4wt.% activated carbon control and NFC containing composites (3-5 wt.%) under 10× optical magnification (scale bar: 100 μm)

A systematic comparison of Figure 2 elucidates the manner in which activated carbon loading governed the interfacial morphology and welding behaviour of the vitrimer when the catalytic environment was held constant. At an activated carbon loading of 3 wt.%, as depicted in Figure 2(a), the welded interface retained a sharply defined fracture boundary, and the welding line remained distinctly visible. This persistence of the crack trace indicates that only limited interfacial wetting and structural reconstruction occurred during the thermal activation. Low loading of carbon-based fillers does not allow the formation of an effective mechanical support network and therefore contributes minimally to the overall structural rigidity of the matrix, as reported by (Syduzzaman *et al*. 2024). Thus, at low activated carbon loading (3 wt.%), the vitrimer network received only limited microstructural reinforcement, as the sparse distribution of rigid carbon particles was insufficient to constrain segmental mobility or provide meaningful dimensional stabilization.

When the activated carbon loading was increased to 4 wt.%, the morphology in Figure 2(d) shows a notable improvement in the coherence of the welded interface, with the welding line becoming less pronounced and the surface appearing smoother and more continuous. Although the interface remained visible, its reduced sharpness and the enhanced surface homogeneity suggest that the matrix was able to undergo partial but more orderly topological rearrangement under these conditions. This indicates that the intermediate filler loading provided a balanced combination of confinement and mobility, thereby allowing bond exchange reactions and segmental motion to proceed in a more coordinated manner along the welded interface. At this loading, the activated carbon particles began to form a more effective stress transfer microstructure, enhancing local stiffness and reducing the amplitude of strain gradients along the fracture plane. Activated carbon, which contains nanostructured and partially graphitic domains, operates as a low dimensional carbon filler; phonons propagate efficiently along the localised graphitic planes but are hindered at pore boundaries, resulting in anisotropic thermal conduction (Aigaje *et al.* 2023; Dai *et al.* 2019; Zhang *et al.* 2022). This directional heat transport behaviour further improves local thermal activation near the crack interface, promoting a more uniform temperature distribution and contributing to the coordinated realignment of the opposing crack faces during welding.

At the highest filler loading in this series, 5 wt.%, the morphology in Figure 2(g) became markedly irregular, with a discontinuous and roughened welded region indicative of pronounced deformation heterogeneity. The suppression of chain mobility at this elevated activated carbon loading aligns with molecular dynamics findings showing that rigid nanoscopic fillers substantially reduce polymer free volume and impose strong interfacial confinement, thereby slowing segmental diffusion and relaxation (Starr *et al.* 2000). The confined polymer matrix exhibited localised roughening, shear deformation traces, and embedded particulate residues. Such features may arise from non-uniform surface flow during thermal activation rather than from void formation or filler debonding. These morphological characteristics collectively reflect the diminished molecular mobility and heightened structural heterogeneity induced by the high filler loading, conditions that restrict dynamic bond interchange and impede the formation of a coherent and continuous healed interface.

Across the NFC loading series, welding behaviour of the vitrimer reflected the synergistic interplay between activated carbon and NFC. This combined mechanism becomes evident when comparing the 3, 4, and 5 wt.% NFC formulations, each demonstrating a different balance between catalytic activity, mobility restriction, and

nanoscale reinforcement within the vitrimer network. The cellulose backbone is stabilised by intrachain hydrogen bonding between hydroxy groups and the ring oxygen atoms of neighbouring glucose units, a structural feature that gives the nanofibers a stiff and linear configuration capable of promoting effective stress transfer in polymer matrices (Collard and Blin 2014; Shaghaleh *et al.* 2018). A distinct improvement in welding performance arose at 4 wt.% NFC, where the catalytic and structural functions of NFC began to work in concert with the thermal-modulating role of activated carbon. As NFC loading increased, a more effective fibrillar network develops within the vitrimer matrix, improving crack-face compatibility. Such intermolecular interactions associated with nanocellulose can generate reversible hydrogen-bonded crosslinking in polymer composites, a mechanism that has been widely exploited in self-healing materials (Lamm *et al.* 2022). Activated carbon, present at moderate levels, improves heat uptake and contributes to a more uniform temperature distribution along the fracture interface, thereby supporting NFC mediated bond exchange without imposing excessive confinement. This balanced interaction is evident in Figure 2(e), where the crack line becomes faint or nearly indistinguishable from the surrounding matrix. The resulting morphology reflects a highly coordinated topological rearrangement in which NFC govern chemical and structural reconfiguration, while activated carbon facilitates thermal activation in a supportive manner.

At 5 wt.% NFC, the welding performance began to deteriorate as excessive nanofiber loading disrupted the stability of the vitrimer network. While the initial addition of filler can enhance thermal stability, further increases in NFC loading may lower the degradation temperature, suggesting that excessive filler disturbs the matrix structure. In addition, hydroxy groups on the NFC surface can form strong hydrogen bonds through hornification, which promotes irreversible agglomeration and reduces the ability of the nanofibers to disperse effectively within the polymer matrix (Beaumont *et al.* 2017). Achieving homogeneous NFC dispersion is widely recognised as essential for optimizing the mechanical and interfacial properties of nanocellulosic composites; however, NFC inherently tend to aggregate through hydrogen bonding and van der Waals interactions, making uniform distribution difficult to maintain (Chu *et al.* 2020). As a result, these agglomerates disrupt the structural continuity of the vitrimer network and produce heterogeneous surface flow, as observed in Figure 2(c), (f), and (i). The formation of such localised clusters creates spatially uneven regions within the vitrimer, where some domains experience excessive confinement while others lack sufficient catalytic activity, ultimately disturbing the coordinated bond exchange required for effective interfacial welding. Moreover, NFC clustering might reduce stress transfer efficiency and limits interfacial cohesion, which further undermines the ability of the vitrimer network to undergo smooth topological rearrangement (Jose *et al.* 2025). As a result, the morphology at 5 wt.% NFC displays incomplete crack closure and irregular surface reconstruction, reflecting a composition where excessive catalytic activation and nanoscale aggregation collectively impair the welding performance.

Effect of Activated Carbon and NFC Loading on the Thermal Stability of EPO-based Vitrimer Composites

Figure 3 shows the thermogravimetric behaviour of the EPO-based vitrimer composites containing different loadings of NFC and activated carbon. All formulations exhibited a two-step thermal degradation pattern, beginning with an initial mass-loss region around 300 to 350 °C, followed by a dominant degradation stage between 350 and 470 °C associated with the rupture of ester linkages and the aliphatic epoxy-derived backbone.

This relatively high temperature for the first degradation event reflects the molecular architecture of EVO networks: their long aliphatic chains and ester functionalities require greater activation energy for scission, which delays the onset of decomposition. Malburet *et al.* (2020) reported that EVO monomers only begin to degrade above 250 °C, supporting the result that EVO-based resin possess intrinsically higher initial thermal stability than conventional petrochemical epoxy monomers. This interpretation aligns with a previous study on a petrochemical epoxy vitrimer, which exhibited three distinct degradation stages, including an early event between 250 to 350 °C attributed to pendant-group scission, followed by aromatic-backbone decomposition (Lee *et al.* 2025a). The absence of this early degradation stage in the EPO vitrimer and the upward shift in its primary decomposition region provide clear evidence that EPO composites can exhibit superior initial thermal stability. This advantage is limited to the onset region, as EPO-based networks continue to generate lower char residues. This behaviour arises from their flexible aliphatic chains and relatively low crosslink density, which limit the formation of thermally stable carbonaceous structures during pyrolysis (Jin and Park 2008).

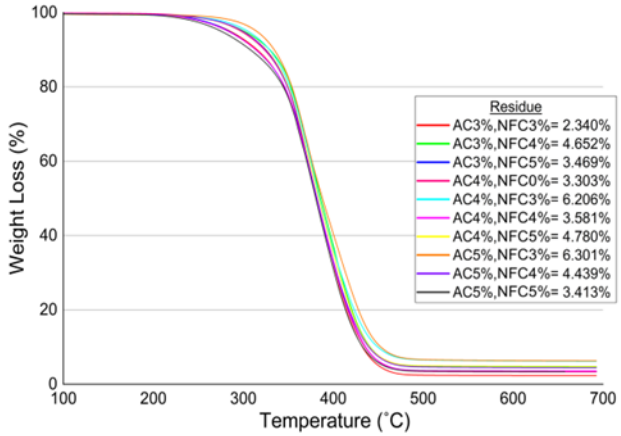

Fig. 3. Effect of NFC and activated carbon loading on the thermal properties of the vitrimer composites

The highest char yields were obtained in the vitrimer composites containing elevated activated carbon loading combined with lower NFC loading, particularly the formulations with 5 wt.% activated carbon and 3 wt.% NFC and with 4 wt.% activated carbon and 3 wt.% NFC, which retained 6.30% and 6.21% residue respectively. Activated carbon is a carbon rich material, partially aromatised material that undergoes minimal mass loss during high temperature pyrolysis and therefore increases the residual mass of the composite (Chin *et al.* 2020). This trend was further reinforced by the behaviour of the PKS-derived activated carbon produced in this study, which exhibited exceptionally high thermal stability, retaining approximately 69% residue even at 1000 °C. This remarkable resistance to thermal degradation can be attributed to the presence of thermally robust oxygen-containing functional groups introduced during the activation process, including anhydrides, lactones, and epoxy-derived C–O–C linkages, which are known to withstand decomposition until considerably elevated temperatures and thereby enhance the char forming capability of bio-derived activated carbons (Lee *et al.* 2018). Collectively, these observations demonstrate that the high temperature stabilisation of the vitrimer composites is strongly governed by the amount of activated carbon in the formulation and by the intrinsic thermal robustness of the PKS-based activated carbon itself.

The effect of NFC addition on the thermal behaviour of the vitrimer composites is clearly evident from the TGA results. At a fixed activated carbon loading of 4 wt.%, the incorporation of NFC led to an approximately 1.9-fold increase in char residue compared with the composite without NFC, indicating a pronounced enhancement in condensed-phase stability. Moreover, NFC loading introduced a distinct influence to the vitrimer network, revealing a clear structure property relationship in the thermal behaviour of the composites. Lower NFC incorporation within the EPO-based vitrimer produced higher char residue, indicating that limited nanofiber content enhanced network cohesion and delayed thermal degradation. Increasing NFC loading introduced a significantly larger surface area and smaller particle dimensions, which generated a higher number of thermally labile end-chains and promoted early-stage decomposition. This trend corresponds to the behaviour described by Yildirim and Shaler (2017), where increased chain end availability in small cellulose particles enhances early thermal breakdown and contributes to elevated char at moderate loadings. However, at highest NFC loading (5 wt.%), the char residue decreased to approximately 3.4 to 4.8%, suggesting a shift in the dominant degradation mechanism. At this point, the intrinsic devolatilisation behaviour of NFC became more influential, where NFC released combustible fragments instead of contributing to char formation. Under dry, hot, and energetic conditions, cellulose combustion generates levoglucosan that rapidly decomposes into CH_4, H_2O, CH_2O, CH_3OH, CO_2, and HCOOH, with major gas evolution occurring between 250 and 400°C which is the pyrolysis region of cellulose, hemicellulose, and lignin (Turku *et al.* 2024). The release of these volatiles accelerates matrix degradation and reduces solid residue, leading to lower char values despite higher solid biomass content (Xu *et al.* 2022). Collectively, these observations reveal a new thermal interplay in NFC reinforced vitrimers, where moderate NFC loadings enhance char yield through end-chain decomposition, while excessive NFC promote volatile driven mass loss and suppresses final residue formation. This behaviour mirrors bioinspired thermal responses commonly seen in natural cellulose structures, where protective charring transitions to volatile release as temperature increases.

Effect of NFC and Activated Carbon Loadings on the Functional Group of Vitrimer Composites

Figure 4 presents the FTIR spectra of the EPO-based vitrimer composites. The strong absorbance band at 1736 cm^{-1} appears consistently across all samples, confirming the formation of an ester-rich network through epoxy-anhydride curing. This ester carbonyl band is characteristic of fatty acid-derived oil structures (Silva *et al.* 2025) and is associated with the generation of new ester linkages during network development (Aliyeva *et al.* 2023). These structures constitute the labile dynamic bonds required for associative transesterification-based vitrimer behavior. This assignment is further supported by the pronounced C–O stretching band at 1179 cm^{-1} (Jawad *et al*. 2016), together with additional C–O absorbances in the 1220 to 1280 cm^{-1} region, which are characteristic of the C–O bonds in ester linkages within the cured network (Smith and Northrop 2014; Vardamides *et al*. 2006). Aside from that, the bands at 2916 cm^{-1} and 2850 cm^{-1} correspond to the asymmetric and symmetric $–CH_2–$ stretching vibrations, respectively (Salih *et al.* 2015), while the absorption near 1470 cm^{-1} is attributed to the bending (deformation) vibration of methyl groups ($–CH_3–$) in the aliphatic backbone (Gheje *et al.* 2025). Together, these bands reflect the aliphatic hydrocarbon backbone of the epoxidised triglyceride structure. Although EPO contains long fatty-acid segments, its triglyceride-based architecture

remains relatively short and less entangled than conventional polymeric vitrimer backbones, highlighting the important role of fillers in enhancing network stiffness and structural integrity.

Across the NFC-containing vitrimer composites, a broad O–H stretching band is observed in the region of 3200 to 3600 cm^{-1}, arising from hydroxy groups in the cured epoxy-anhydride network together with contributions from cellulose surface –OH functionalities. A feature near 3836 cm^{-1} becomes apparent after NFC incorporation and may be attributed to additional hydroxy environments associated with the cellulose filler (Wang *et al.* 2018). These hydroxy groups enhance filler-matrix cohesion through interfacial hydrogen bonding, contributing to mechanical reinforcement (Karoki *et al.* 2025). Nevertheless, overly high NFC loading can be detrimental. The formulation containing 4 wt.% NFC exhibited several distinguishable O–H stretching components in the higher wavenumber region, with features around 3525, 3564, and 3801 cm^{-1}, suggesting a balanced hydroxy interaction environment and effective interfacial organisation. In contrast, when the NFC loading was increased to 5 wt.%, these sharper hydroxy bands became less resolved or disappeared and the overall O–H envelope appeared more broadened, implying increased hydroxy clustering and partial filler aggregation at excessive loading. Such aggregation can locally stiffen the network and reduce chain mobility, consistent with the rougher healed interface observed for the highest NFC formulation (Figure 2(f)), thereby limiting efficient network reorganisation during self-healing.

These hydroxy functionalities not only participate in interfacial hydrogen bonding with the surrounding polymer matrix but also act as reactive sites within the dynamic covalent network. In epoxy-anhydride composites, curing proceeds through the ring opening reaction between epoxide groups and cyclic anhydrides, generating repeating units containing both ester linkages and alcohol groups through reaction pathway (a). The coexistence of these functionalities is essential for vitrimer behaviour. At elevated temperatures, the alcohol groups can react with neighbouring ester linkages through catalytic ester-alcohol transesterification, as represented by reaction pathway (b) (Denissen *et al.* 2016). In the present composite, citric acid acts as an acid catalyst that promotes this exchange process. Under catalytic conditions, the ester carbonyl becomes activated, enabling nucleophilic attack by a neighbouring hydroxy group through an alcoholysis pathway, which results in the formation of a new ester linkage and the release of another alcohol molecule (Su *et al.* 2024). Because bond formation precedes bond cleavage, the overall crosslink density of the network is maintained during the exchange. Consequently, this dynamic covalent mechanism allows continuous network rearrangement under thermal activation, providing the molecular basis for the welding behaviour observed in the EPO-based vitrimer composites.

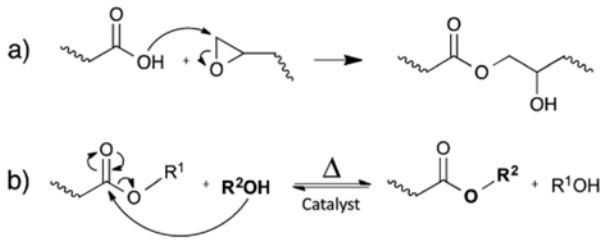

Meanwhile, Figure 4 also compares vitrimer composites with varying activated carbon loadings, both in the absence and presence of NFC.

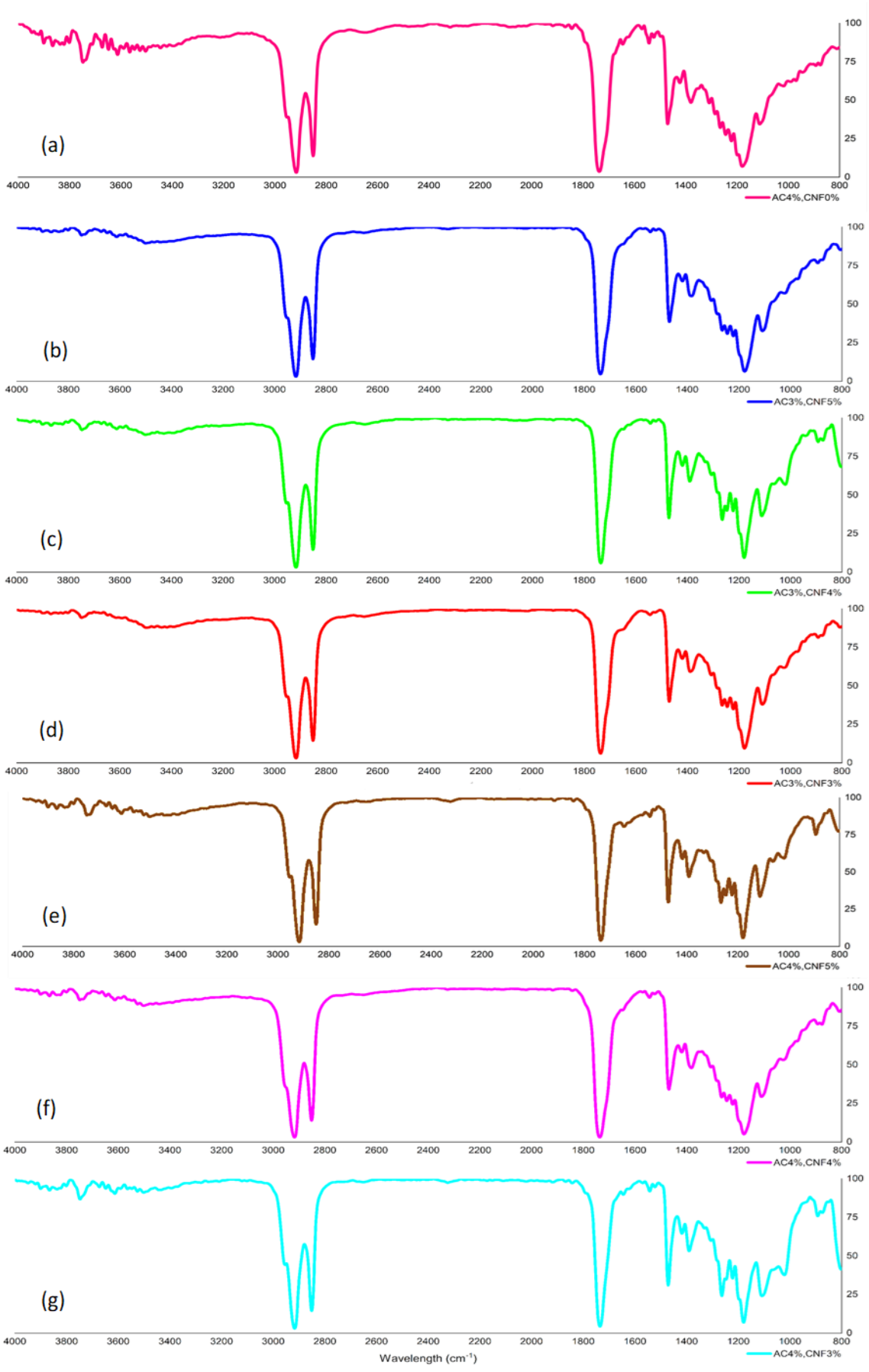
(a)
AC4%,CNF0%
(b)
AC3%,CNF5%
(c)
AC3%,CNF4%
(d)
AC3%,CNF3%
(e)
AC4%,CNF5%
(f)
AC4%,CNF4%
(g)
AC4%,CNF3%
4000 3800 3600 3400 3200 3000 2800 2600 2400 2200 2000 1800 1600 1400 1200 1000 800
100 75 50 25 0
Wavelength (cm-1)

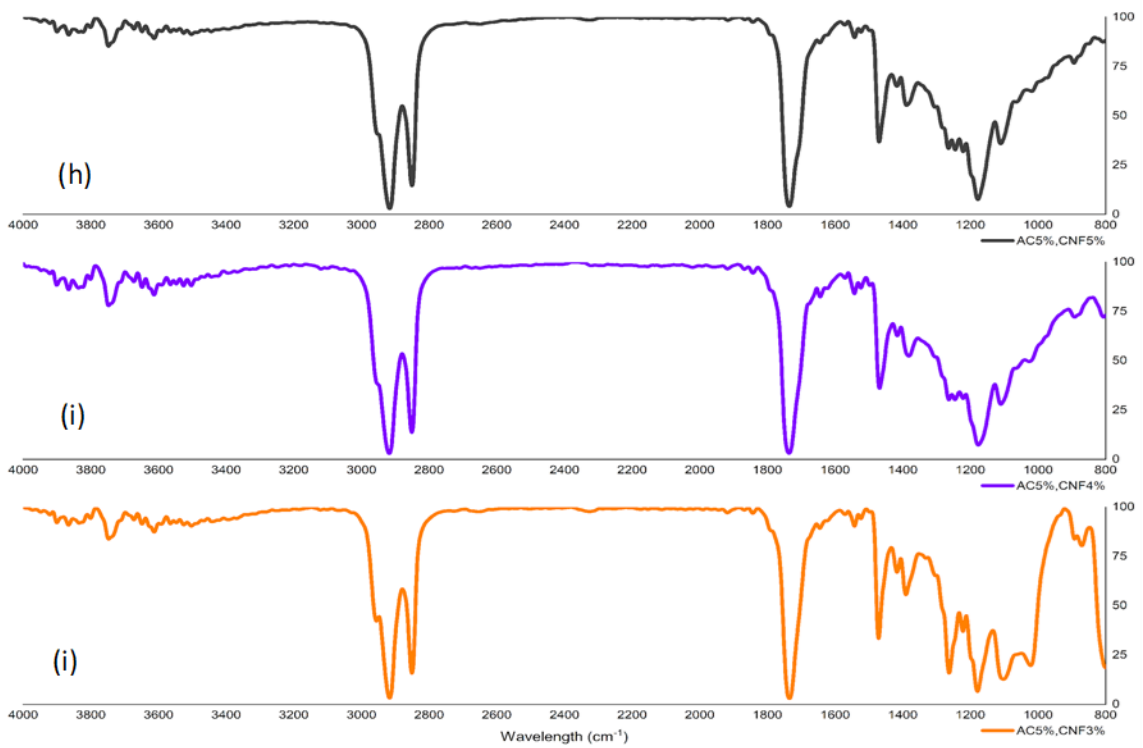

Fig. 4. FTIR spectra of vitrimer composites with varying activated carbon and NFC loadings: (a) AC4%/N0%, (b) AC3%/N5%, (c) AC3%/N4%, (d) AC3%/N3%, (e) AC4%/N5%, (f) AC4%/N4%, (g) AC4%/N3%, (h) AC5%/N5%, (i) AC5%/N4%, and (j) AC5%/N3%.

In the mid-IR region of the vitrimer formulation containing activated carbon only, the band at 1843 cm^{-1} is assigned to the asymmetric C=O stretching vibration of the five member cyclic anhydride ring (Zhang *et al.* 2025). Additionally, bands at 2085 cm^{-1}, 2317 cm^{-1}, and 1569 cm^{-1} are associated with activated carbon surface related species and graphitic aromatic (C=C) structures (Aribam *et al.* 2025; Cherik and Louhab 2017; Rajasekaran and Raghavan 2022). These activated carbon related features become less distinguishable upon the incorporation of NFC into the vitrimer composites, which may be attributed to masking by the stronger polymer and cellulose absorbance bands.

Effect of Formulation Variables on the Solvent Resistance of EPO-based Vitrimer Composites

In practical applications, vitrimer materials must exhibit strong solvent resistance during service while retaining the potential for controlled solvolysis under specific end-of-life conditions (Xia *et al.* 2024). Therefore, the solvent resistance and degradation behaviour of the palm oil derived epoxy vitrimer composites were evaluated based on swelling ratio, gel content, and visual observations after 24 h of solvent immersion, as presented in Table 2 and Figure 5, to assess network stability and recyclability. The swelling ratio reflects the extent of solvent uptake and network expansion, indicating network density and solvent resistance, while gel content represents the insoluble fraction, reflecting the degree of crosslinking and structural integrity of the network. As shown in Table 2, all formulations exhibited very low swelling values (<6%), confirming the formation of a chemically stable vitrimer network. In contrast, many synthetic epoxy composites, particularly DGEBA-based vitrimers with lower effective crosslink density or

network defects, can exhibit swelling ratios exceeding 100% in aggressive organic solvents due to extensive chain plasticization and solvent penetration (Lee *et al.* 2025a). In the present composite, epoxy anhydride curing between EPO and HHMPA forms an ester-rich crosslinked network through ring opening reactions that generate ester linkages and hydroxy groups, contributing to the observed solvent resistance (Khairkkar *et al*. 2025; Paramarta *et al.* 2016). This behaviour is further supported by the molecular structure of vegetable oil-based epoxies, where monounsaturated fatty acid segments and long aliphatic chains promote flexible yet stable network architectures (Li *et al.* 2026) while reducing solvent affinity, resulting in improved chemical stability compared with conventional petroleum-based epoxy composites (Chong *et al.* 2021).

Furthermore, the presence of NFC and activated carbon introduces additional physical constraints that reduce free volume and create tortuous diffusion pathways, effectively restricting solvent penetration. As a result, solvent uptake is confined to minor network expansion rather than large scale swelling, explaining why the swelling ratios remain well below 6% for the EPO-based vitrimer, in contrast to the excessive swelling commonly observed in conventional synthetic epoxy materials. In particular, water (H_2O) induces negligible swelling across all samples, which is further confirmed by the absence of dimensional or colour changes in the immersed specimens (refer to Figure 5). This behaviour indicates that water interaction is largely confined to surface absorption and is insensitive to variations in activated carbon and NFC loadings, reflecting the limited affinity of the vitrimer network toward water. Slightly higher swelling is observed in methanol and acetone, consistent with their small molecular size and moderate polarity, which allow partial diffusion into the polymer matrix without causing significant network disruption (Momin *et al.* 2025).

Table 2. Swelling Ratio and Gel Content of Vitrimer Composites at Different Activated Carbon and NFC Loadings in Various Solvents

Swelling Rate (%)										
Solvent	A_4	A_3/N_3	A_3/N_4	A_3/N_5	A_4/N_3	A_4/N_4	A_4/N_5	A_5/N_3	A_5/N_4	A_5/N_5
H_2O	0	0	0	0	0	0	0	0	0	0
Toluene	1.67	2.25	2.25	1.80	0.75	2.00	2.50	2.00	1.50	2.50
Methanol	0.25	0.25	0	0	0.20	0.17	0	0	0	0
1,4-Dioxane	1.40	2.75	2.25	2.40	1.75	3.00	1.25	1.67	2.00	3.25
Ethyl Acetate	2.00	1.83	1.00	1.50	0.60	1.75	0.40	0.25	1.25	1.80
Chloroform	3.25	2.80	5.20	3.20	5.00	2.75	1.60	1.33	3.40	5.60
Acetone	0	1.00	0.50	1.00	0.50	0.50	0.60	0.25	0.33	0.57
Gel Content (%)										
Solvent	A_4	A_3/N_3	A_3/N_4	A_3/N_5	A_4/N_3	A_4/N_4	A_4/N_5	A_5/N_3	A_5/N_4	A_5/N_5
H_2O	100	100	100	100	100	100	100	100	100	100
Toluene	45	75	55	30	55	75	60	75	75	40
Methanol	20	35	25	15	25	35	32	35	37	20
1,4-Dioxane	60	100	75	40	75	100	75	100	100	50
Ethyl Acetate	35	60	45	25	45	60	56	60	60	30
Chloroform	50	65	80	35	65	85	60	74	88	45
Acetone	30	55	40	22	40	55	35	55	55	30

Note: A_x/N_y denotes composites containing x wt.% activated carbon (A) and y wt.% NFC (N). (A_3/N_4 represents a formulation with 3 wt.% activated carbon and 4 wt.% NFC)

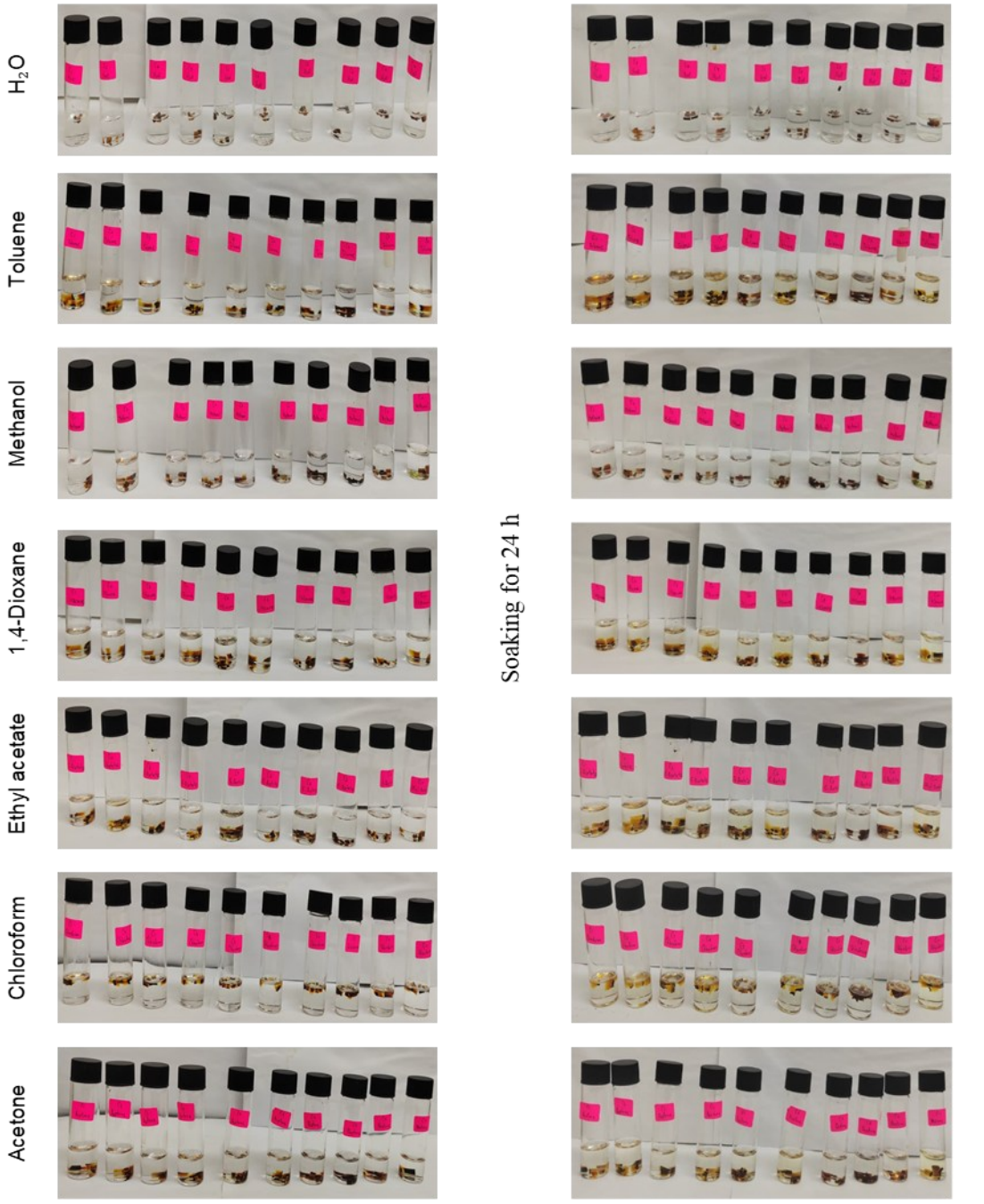

Fig. 5. Digital photograph of EPO-based vitrimer soaked in different solvents

In contrast, chloroform and 1,4-dioxane induce noticeably higher swelling, clearly highlighting the influence of formulation on solvent resistance. This trend is evident both quantitatively in the swelling rate data and visually through increased sample softening and solvent coloration, as shown in Table 2. The stronger swelling response in these solvents arises from their higher affinity toward epoxy-based networks, making them effective probes for assessing network integrity. Importantly, increasing activated carbon loading leads to a consistent reduction in swelling in chloroform and 1,4-dioxane, demonstrating that activated carbon enhances solvent resistance by physically restricting polymer chain mobility and increasing the tortuosity of solvent diffusion pathways. Similarly, formulations containing higher NFC loading (5 wt.%) generally exhibit lower swelling than those with 3 to 4 wt.% NFC, reflecting improved network compactness and more effective chain immobilization. The slightly higher swelling observed at intermediate NFC loading can be attributed to localised heterogeneity or dispersion effects, as also suggested by subtle visual differences among the samples.

The gel content results presented in Table 2 further highlight the dominant role of NFC loading in governing the solvent resistance and network integrity of the palm oil derived epoxy vitrimer composites. While all samples remain insoluble in the tested solvents, clear NFC dependent variations in gel content were observed. Formulations containing higher NFC loading generally exhibited higher gel content across most solvents, indicating a greater fraction of polymer chains were effectively incorporated into the EPO-based vitrimer network. This behaviour reflects the reinforcing role of NFC, which promotes physical entanglement and interfacial interactions with the epoxy matrix, thereby restricting chain mobility and reducing the extractable sol fraction. In aggressive solvents such as chloroform and 1,4-dioxane, samples with lower NFC loading showed a more pronounced reduction in gel content, suggesting that a less reinforced network allows partial extraction of loosely bound chains. In contrast, increasing NFC loading mitigates this effect, maintaining higher gel content even under strong solvent exposure. This NFC-dependent trend correlates well with the swelling results in Table 2, where higher NFC loading corresponded to reduced swelling. The photographic evidence in Figure 5 further supports this interpretation: samples with higher NFC loading retained their shape and colour after solvent immersion, whereas those with lower NFC loading exhibited slight softening or edge deformation, particularly in chloroform. Overall, these results demonstrate that NFC played a critical role in enhancing network compactness, stabilizing the vitrimer structure, and improving solvent resistance in palm oil derived epoxy vitrimer composites.

Morphological Analysis of Vitrimer Composites

Based on the chemical resistance results discussed in the previous section, vitrimer composites reinforced with NFC and activated carbon exhibited notable stability under chemical exposure. To further elucidate the structural features responsible for this behaviour, morphological analysis was performed using FESEM to examine the surface and interfacial morphologies of the vitrimer composites, with particular attention to filler distribution and matrix continuity. The hybrid composite containing 4 wt.% NFC and 4 wt.% activated carbon was analysed (Figure 7), while a vitrimer containing only 4 wt.% activated carbon was examined as a reference sample (Figure 6). A comparison of these samples revealed clear differences in interfacial architecture between the activated carbon only composite and the hybrid NFC and activated carbon composites, highlighting the role of NFC in improving interfacial connectivity within the vitrimer matrix. These structural

differences correlated with the welding-assisted self-healing behaviour observed in vitrimer composites. Dynamic covalent chemistries enable vitrimer segments to be reconnected through welding after curing *via* thermally activated bond exchange (Shi *et al.* 2023; Wu *et al.* 2023). In vitrimer composites, topological rearrangement at elevated temperatures allows previously cured materials to be rejoined under heat and pressure, effectively restoring interfacial continuity despite limited matrix flow (Masten-davies *et al.* 2025; Vashchuk and Kobzar 2022). This welding capability therefore contributes to the durability of vitrimer composites by enabling repeated interfacial repair.

The interface in the activated carbon only vitrimer (Figure 6(b)) was characterised by a distinct linear feature accompanied by interstitial regions, indicating limited continuity between adjoining vitrimer domains. This morphology reflects the influence of rigid particulate fillers on polymer chain interdiffusion and interfacial reconnection, processes that are required for effective welding or self-healing in polymer composites. The restricted interfacial continuity is further evident in Figure 6(c), where localised gaps appear between activated carbon particles and the surrounding vitrimer matrix, indicating incomplete polymer and filler contact and constrained local chain mobility during thermal activation (Dubey *et al.* 2020). The microstructural origin of this behavior is revealed in Fig. 6(d), which shows exposed activated carbon platelets with a lamellar, flake like morphology arising from weak interactions between overlapping carbon sheets. When incorporated into a rigid amorphous vitrimer network, these loosely stacked carbon structures disrupt uniform matrix penetration and dense polymer packing, generating regions of reduced network continuity (Kotan and Bayrakçeken 2022).

In contrast, the hybrid vitrimer composite exhibited a fundamentally different interfacial morphology. At the same magnification, Figure 7(b) shows no discernible interface line, indicating effective structural continuity between adjoining vitrimer regions at the microscopic scale. This absence of a visible boundary reflects enhanced interfacial connectivity associated with the presence of NFC, which promotes polymer chain mobility and network interpenetration during thermal activation. As polymer chains become mobile and interdiffuse across the interface, intimate contact between the vitrimer matrix and NFC are established, enabling the development of interfacial interactions (Ge *et al*. 2012). This process is evident in Figure 7(c), where NFC particles were distributed within the interfacial region and extended between activated carbon particles and the vitrimer matrix, occupying regions that appear as gaps in the activated carbon only vitrimer and promoting local network continuity. The resulting interfacial reorganization is further manifested in Figure 7(d), which reveals a compact, crumpled lamellar morphology dominated by activated carbon platelets that are folded and constrained within the vitrimer matrix. This morphology arises from thermally activated rearrangement of lamellar carbon sheets under matrix confinement, where the presence of NFC and the surrounding vitrimer network suppress platelet separation and pull-out, favoring folding and compaction instead. Such confinement maintains intimate matrix filler contact and prevents the formation of interfacial voids, allowing the interfacial region to behave as a consolidated, load-bearing zone. Consequently, polymer chain interdiffusion and dynamic covalent bond exchange can proceed across the interface without disruption, leading to the formation of an interpenetrating polymer network-like interfacial structure in which the vitrimer network and NFC associated polymer regions are topologically intertwined (Feng *et al.* 2025). This stabilised interfacial architecture provides a microstructural basis for the disappearance of a distinct interface line and supports effective welding assisted self-healing behavior in the hybrid vitrimer composite.

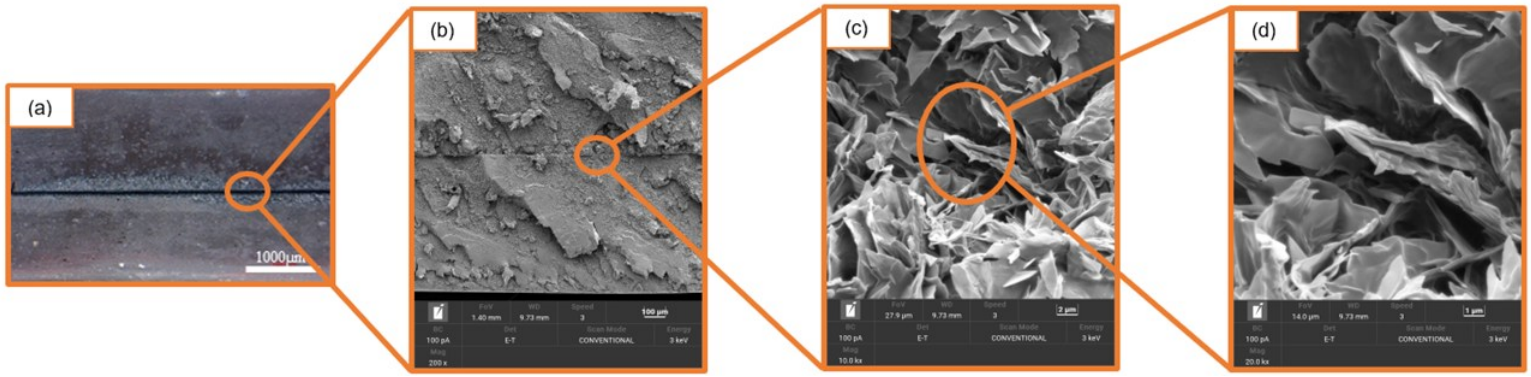

Fig. 6. Surface morphology of the welded vitrimer composite containing 4 wt% activated carbon.
(a) Optical microscopy image of the welding line region formed at the interface between two vitrimer samples after thermal welding.
(b) Scanning electron microscopy image of the welding surface at higher magnification.
(c) Higher magnification view of the interfacial region between the vitrimer matrix and activated carbon particles along the welding line.
(d) Microstructural features of the vitrimer matrix and activated carbon in the welded region.

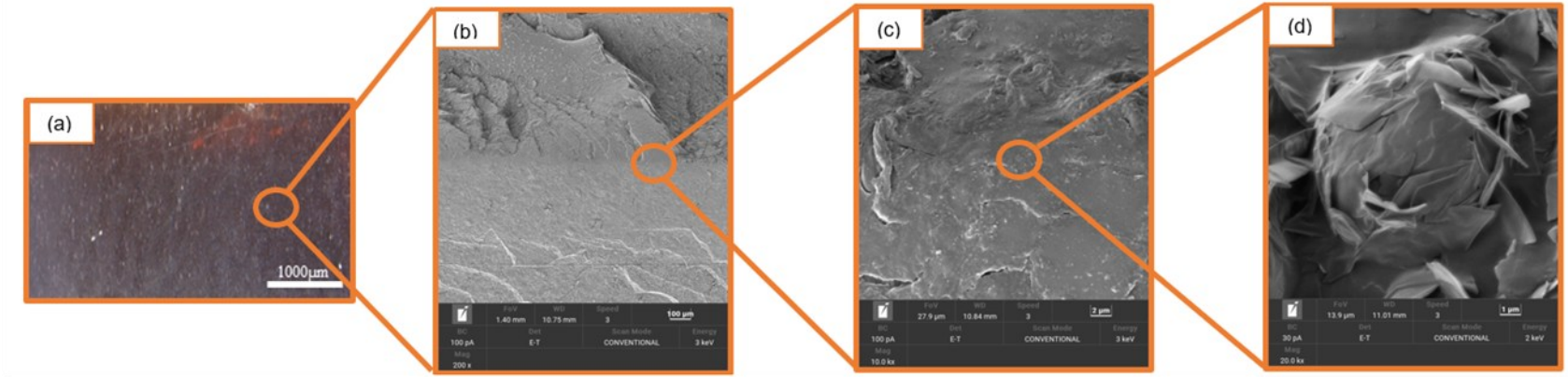

Fig. 7. Surface morphology of the welded vitrimer composite containing 4 wt.% activated carbon and 4 wt.% cellulose nanofibers.
(a) Optical microscopy image of the welding line region at the interface between two vitrimer samples after thermal welding.
(b) Scanning electron microscopy image of the welding surface at higher magnification.
(c) Higher magnification view of the interfacial region between the vitrimer matrix, activated carbon, and NFC along the welding line.
(d) Microstructural features of the vitrimer matrix and fillers in the welded region.

To rationalise these interfacial observations, Figure 8 summarises the integrated chemical mechanical mechanisms governing self-healing in the present vitrimer composites. As illustrated in Figure 8(a), the curing of EPO proceeds through epoxy anhydride ring opening reactions with HHMPA and epoxy acid reactions involving citric acid. The epoxy ring opening reactions between EPO, HHMPA, and citric acid form β-hydroxy ester linkages, where the hydroxy groups originate from the epoxy ring opening of EPO, while the ester bonds arise from reactions between the epoxide groups and the anhydride and carboxylic acid groups of HHMPA and citric acid. Both epoxy-anhydride and epoxy-acid reactions generate β-hydroxy ester linkages, allowing the two curing pathways to coexist within the same crosslinked network and enabling subsequent transesterification exchange reactions characteristic of vitrimer composite. The occurrence of the curing reaction is supported by FTIR analysis, as shown in Figure 8 (c). The spectrum of pure EPO exhibits characteristic absorption peaks at approximately 912 cm^{-1} and 827-829 cm^{-1}, corresponding to the C–O–C stretching vibration of the oxirane ring, confirming the presence of epoxy groups in the EPO structure *(Dan et al. 2014; Sinaga et al.* 2024). After curing with HHMPA and citric acid, the intensity of these epoxy peaks significantly decreases, indicating that the epoxide groups have been consumed during the ring opening reactions. At the same time, the carbonyl stretching band at ~1734 cm^{-1}, characteristic of the C=O vibration of ester groups, becomes more pronounced in the cured samples (refer Figure 4). The reduction of the oxirane peaks together with the increase of the ester carbonyl absorption confirms the cleavage of the epoxy ring and the formation of ester linkages during the curing process(Vanags *et al.* 2018).

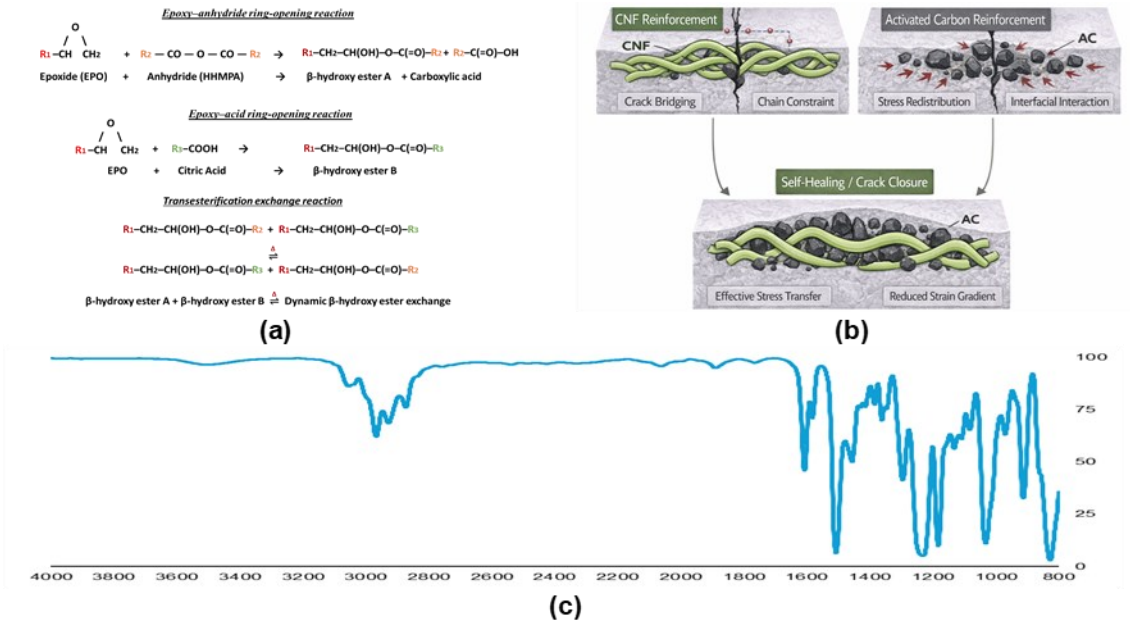

Fig. 8. (a) Chemical curing reactions illustrating the vitrimer bond exchange mechanism in the EPO system. **(b)** Mechanical reinforcement effects of NFC and activated carbon in the self-healing EPO-based composites. **(c)** FTIR spectrum of pure epoxidised palm oil (EPO)

In addition to the chemical curing mechanism, Figure 8(b) illustrates the mechanical reinforcement provided by NFC and activated carbon in the vitrimer composite. These fillers do not participate in the chemical curing reactions and therefore do not form new covalent bonds with the vitrimer network. Instead, they are physically

incorporated into the polymer matrix and contribute through mechanical reinforcement. The fibrous structure of NFC facilitates crack bridging and chain constraint within the matrix, helping to maintain contact between fractured surfaces during deformation. Meanwhile, activated carbon particles act as rigid fillers that redistribute local stresses within the composite and improve stress transfer. The combined effect of NFC and activated carbon assists crack closure and reduces strain localisation within the material. Consequently, the synergy between dynamic vitrimer bond exchange and filler induced mechanical reinforcement contributes to the enhanced self-healing performance observed in the EPO-based composites.

Reprocessing Behaviour of Vitrimer Composites

Vitrimers represent a more sustainable alternative to conventional polymers due to their inherent recyclability, repairability, and stable mechanical performance. To facilitate the reuse of vitrimer composites after their service life, it is desirable that the material can be recovered and reprocessed while maintaining its structural integrity (Amin 2026; Fuchs *et al.* 2026). In this study, the reprocessing behaviour of the vitrimer composites was evaluated through DMA and creep-recovery measurements.

Effect of Activated Carbon and NFC Loading on the Storage Modulus of Vitrimer Composite

As shown in Figure 9(a-b), the storage modulus of the EPO-based vitrimer composites decreases progressively with increasing temperature, reflecting the thermal softening behaviour typical of aliphatic epoxy networks derived from EPO. This reduction is associated with the molecular structure of the palm oil derived polymer network, in which saturated fatty acid segments are incorporated as flexible side chains along the backbone. These aliphatic segments enhance chain mobility and lower the glass transition temperature (T_g), leading to a gradual decrease in stiffness as the temperature increases (Stavila *et al.* 2023).

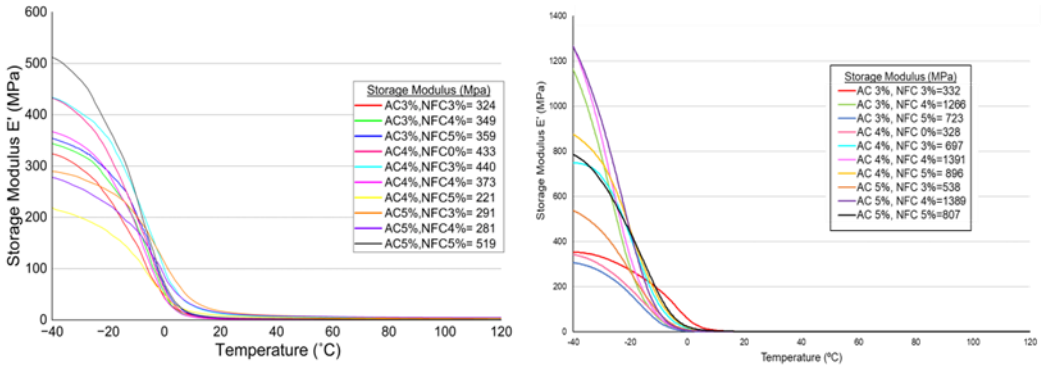

Fig. 9. Effect of activated carbon and NFC loading on the storage modulus of EPO-based vitrimer composites: **(a)** pristine samples and **(b)** reprocessed samples

For the vitrimer containing activated carbon only, the storage modulus remained relatively limited, reflecting the localised constraint imposed by particulate fillers. In contrast, the vitrimer incorporating 4 wt.% activated carbon together with 4% of NFC exhibited a higher storage modulus, indicating more effective restriction of polymer chain motion. This enhancement is associated with strong interfacial interactions between the

vitrimer matrix and NFC, which hinder segmental mobility and reduce deformation under dynamic loading (Gan *et al.* 2020; Wang *et al.* 2022). At the same composition, the composite containing NFC also shows improved thermal stability (refer Figure 3), indicating increased resistance to chain scission and enhanced retention of the condensed phase. The simultaneous increase in storage modulus and char residue upon the addition of NFC suggests that thermal stability and mechanical stiffness are coupled through the restricted mobility of polymer chains introduced by the nanofibrillar reinforcement.

Figure 9(a) illustrates that the activated carbon exerted the strongest control over stiffness. When the NFC loading was fixed at 3 wt.%, increasing the activated carbon loading from 3 to 4 wt.% produced a pronounced increase in storage modulus, indicating the formation of a more rigid network structure. This enhancement is attributed to the introduction of additional rigid carbonaceous domains at higher loading, which restrict segmental motion of the polymer chains and improve stress transfer within the vitrimer matrix. Such restriction of chain mobility arises from interactions between activated carbon surfaces and the polymer backbone, which suppress local molecular rearrangements and increase the overall stiffness of the composite (Nuryanta *et al.* 2023). The higher storage modulus observed for the formulation containing 4 wt.% activated carbon is in agreement with its lower swelling behaviour. With NFC fixed at 3 wt.%, the swelling ratio decreased from 5% for 3 wt.% activated carbon to 2.80% for 4 wt.% activated carbon, suggesting a more compact and constrained polymer network. In polymer networks, reduced swelling generally reflects increased network constraint, as materials with higher crosslink density exhibit lower swelling ratios due to restricted expansion of polymer chains in the solvent (Sairi *et al.* 2025).

Figure 9(b) displays a notable improvement in storage modulus is observed for the reprocessed EPO-based vitrimer composites containing NFC compared with their pristine counterparts. The most significant enhancement occurred in vitrimer containing 4 wt.% NFC, where the storage modulus increased by approximately two to four times after reprocessing, indicating that the nanofibrillar framework formed at this loading provided effective reinforcement during vitrimer network rearrangement. This behaviour contrasts with conventional thermosetting polymers, which are difficult to recycle because their permanent covalent crosslinked networks prevent melt processing and structural rearrangement once the network is formed (Li *et al.* 2021). Dynamic covalent bonds enable the network to rearrange during thermal reprocessing while preserving overall connectivity, allowing well dispersed NFC to act as an effective reinforcing phase within the vitrimer matrix. Assisted by ultrasonic mixing, the NFC form an interconnected nanofibrillar framework that enhances interfacial bonding with the epoxy matrix and partially immobilizes nearby polymer chains, thereby increasing local stiffness and resistance to elastic deformation (Balakrishnan *et al.* 2017; Rana and Gupta 2021). Moreover, activated carbon contributes through its high surface area and oxygen containing functional groups, promoting interfacial adhesion and efficient load transfer within the composite network (Lee *et al.* 2025a). The synergistic interaction between the rigid activated carbon domains and the NFC nanofibrillar scaffold stabilizes the reorganised vitrimer structure and enables the composite to retain significantly higher stiffness after reprocessing. In contrast, the vitrimer reinforced solely with activated carbon shows a reduction in storage modulus after reprocessing, as the absence of a nanofibrillar reinforcement framework limits the composite's ability to maintain stiffness during thermal recycling.

As shown in Figure 9(a), when activated carbon was fixed at 3 wt.%, increasing NFC loading led to a gradual rise in storage modulus from 324 MPa at 3 wt.% NFC to 349 MPa at 4 wt.% and 359 MPa at 5 wt.%, indicating progressively stronger restriction of molecular mobility due to the formation of hydrogen bonded nanofibrillar domains. Across all formulations, the composite containing 5 wt.% activated carbon and 5 wt.% NFC exhibited the highest stiffness, reaching 519 MPa, reflecting the combined reinforcement from the carbonaceous filler framework and the interconnected NFC network that enhances load transfer within the matrix. However, such a highly constrained structure may also promote a more brittle response due to excessive filler-filler interactions and reduced chain mobility. In contrast, the behaviour after reprocessing (Figure 9(b)) shows a stronger dependence on filler composition. When NFC loading was maintained at 4 wt.%, increasing activated carbon from 3 to 4 wt.% resulted in a noticeable increase in storage modulus, suggesting that additional rigid carbon domains further restrict segmental motion and reinforce the NFC network. However, further increasing activated carbon to 5 wt.% did not produce proportional improvement. This behaviour may arise from the development of a filler network at high filler loading, where enhanced filler-filler interactions alter the dynamic viscoelastic response of the composite and contribute to the modulus at low strains (Bokobza 2023). This difference between the pristine and reprocessed composites suggest that thermal reprocessing alters the internal filler distribution and network organization of the vitrimer matrix.

Effect of NFC and Activated Carbon Loadings on the Damping Factor of Vitrimer Composites

Table 3 shows the effect of activated carbon and NFC loading on the glass transition region (T_g) of the EPO-based vitrimer composites. All formulations exhibited a single dominant tan δ peak between approximately 1 and 8 °C, corresponding to the T_g where the vitrimer network transitions from a rigid, glassy state to a more mobile, rubbery phase that enables segmental motion and molecular rearrangement (Karatrantos *et al.* 2024). When the activated carbon loading was fixed at 3 wt.%, increasing NFC loading from 3 to 5 wt.% raised T_g from 1.47 to 7.48 °C, indicating progressively stronger restriction of segmental motion introduced by the NFC fibrillar domains.

Table 3. Glass Transition Region of EPO-based Vitrimer Composites

Activated carbon loading (wt.%)	NFC Loading (wt.%)	Glass Transition (T_g) (pristine sample)	Glass Transition (T_g) (reprocessed sample)
3	3	1.47ºC	8.22
3	4	6.67ºC	-2.28
3	5	7.48ºC	-3.60
4	-	6.43ºC	-1.73
4	3	4.14ºC	-0.62
4	4	6.91ºC	-2.31
4	5	1.81ºC	0.28
5	3	5.30ºC	-1.02
5	4	5.45ºC	-0.63
5	5	6.18ºC	0.79

A similar trend was observed at 4 wt.% activated carbon, where T_g increased from 4.14°C at 3 wt.% NFC to 6.91°C at 4 wt.% NFC, reflecting enhanced interfacial

interactions between the fillers and the vitrimer matrix. However, further increasing NFC loading to 5 wt.% caused T_g to decrease sharply to 1.81°C, suggesting that excessive NFC may disrupt optimal dispersion and reduce mobility control within the network. In contrast, the reprocessed samples exhibited T_g values closer to 0 °C, indicating relatively high segmental mobility within the predominantly amorphous vitrimer structure after thermal recycling (Krishnan *et al.* 2022).

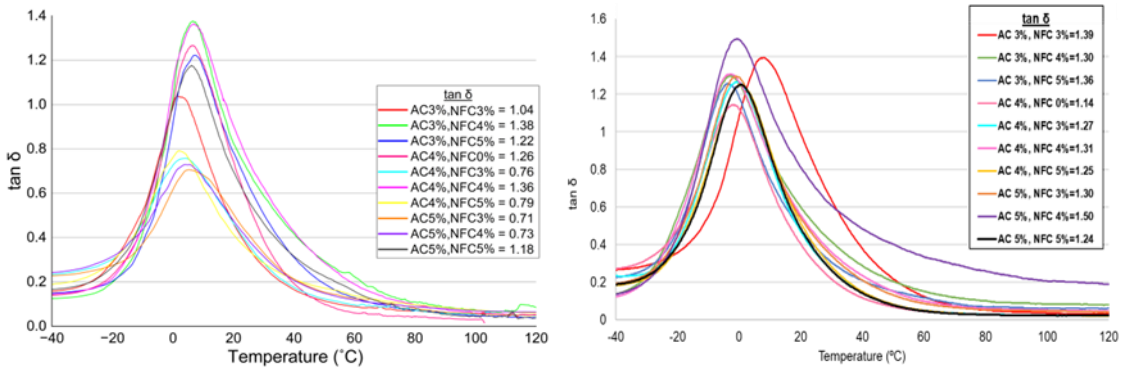

Fig. 10. Effect of activated carbon and NFC loading on the damping factors of EPO-based vitrimer composites: **(a)** pristine samples and **(b)** reprocessed samples.

When the activated carbon loading was fixed at 4 wt.%, a clear progression in the damping response was observed with increasing NFC loading, as shown in Figure 10(a). The composite containing 4 wt.% NFC exhibited the highest tan δ within this series (tan δ ≈ 1.36), indicating enhanced molecular relaxation and energy dissipation during the glass-transition process. This behaviour can be attributed to the structural characteristics of NFC: their high aspect ratio enables efficient redistribution of local stresses, while their semi-crystalline fibrillar structure restricts large-scale chain mobility and promotes stronger interactions with the surrounding epoxy matrix (Hu *et al*. 2021; Jose *et al.* 2025). In combination with the thermally responsive microdomains introduced by activated carbon, this hybrid filler formulation creates a balanced viscoelastic environment that facilitates controlled network rearrangement under thermal activation. Consequently, the formulation containing 4 wt.% activated carbon and 4 wt.% NFC exhibits a seamless healing interface, indicating effective molecular reorganisation and welding (Figure 2(e)).

In contrast, the composite containing 3 wt.% activated carbon and 4 wt.% NFC showed the highest overall tan δ among all formulations (≈1.38), suggesting a larger viscous contribution to the viscoelastic response. Materials with elevated viscous elasticity typically display higher damping due to increased molecular friction during thermal softening (Bertolo *et al*. 2023; Wang *et al*. 2024). Under these conditions, the vitrimer network becomes overly compliant and more susceptible to time-dependent deformation. This effect is consistent with the morphology observed in Figure 2(b), where elongated streaks and sagged surface features indicate creep-like viscoelastic flow during thermal activation. Therefore, while moderate damping promotes interfacial rearrangement, excessive damping can hinder controlled crack closure. In comparison, the balanced viscoelastic behaviour achieved at 4 wt.% activated carbon and 4 wt.% NFC enabled more effective interfacial welding.

As shown in Figure 10(b), the reprocessed vitrimer composites exhibited higher damping behaviour compared with the pristine samples, as indicated by the increased tan

δ values. This enhancement may be associated with structural modifications occurring during thermal recycling. Elevated recycling temperatures can promote additional reactions such as catalytic ring opening polymerization, which alter the network architecture of the vitrimer composite and influence its viscoelastic response (Jing *et al*. 2022). In addition, variations in activated carbon and NFC loading also influence the damping response of the reprocessed composites. Based on Figure 10(b), the composite containing 5 wt.% activated carbon and 4 wt.% NFC exhibited the highest tan δ peak, indicating more effective energy dissipation. The incorporation of nanomaterials can significantly increase the extent of the filler matrix interfacial region, which enhances energy dissipation within the composite (Gong *et al.* 2022). In particular, the presence of NFC can introduce stick-slip friction at the filler matrix interface, which contributes to improved damping behaviour (Jang *et al*. 2012). However, when the NFC loading increases to 5 wt.%, the damping peak slightly decreases, which may be associated with partial nanofiber aggregation that limits effective interfacial interaction within the composite structure.

Effect of NFC and Activated Carbon Loadings on the Creep-Recovery Behaviour of Vitrimer Composites

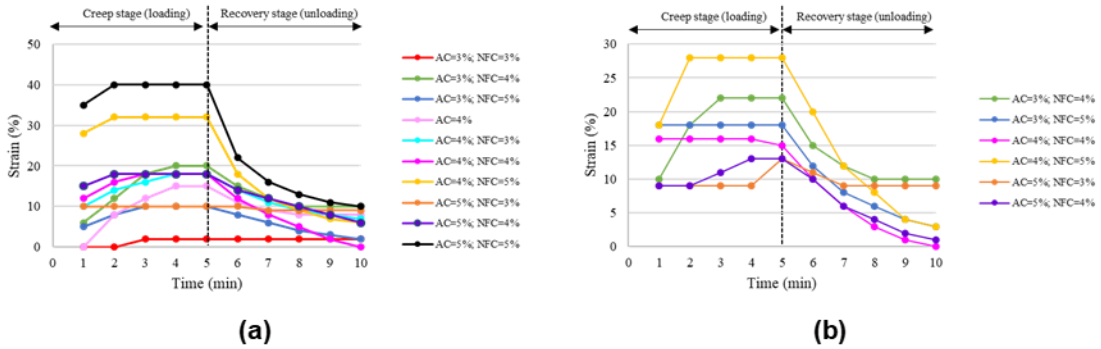

Fig. 11. Creep-recovery curves of vitrimer composites with different NFC and activated carbon loadings in the **(a)** pristine and **(b)** reprocessed states

Unlike permanently crosslinked epoxy thermosets, which exhibit nearly zero creep (*i.e.*, little or no change in strain under constant load or stress), vitrimer materials may undergo time-dependent deformation due to their dynamic bond exchange mechanism (Perego and Khabaz 2022). Consequently, achieving thermoset-like creep resistance remains a key challenge, making creep testing important for evaluating their mechanical stability (Singh *et al.* 2024). The creep-recovery behaviour of the vitrimer composites (Figure 11(a): pristine; Figure 11(b): reprocessed) is influenced by the combined effects of NFC and activated carbon loading. Under constant stress at room temperature, all compositions showed noticeable creep deformation, reflecting the viscoelastic nature of the dynamic vitrimer network. After unloading, residual strain remained in most samples, indicating incomplete recovery caused by stress relaxation and network topology rearrangement enabled by dynamic covalent bond exchange (Roig *et al.* 2023). This bond reshuffling allows stress dissipation through network reconfiguration but may also limit full strain recovery.

This network rearrangement was further reflected in the mechanical performance after recovery. As shown in Figure11(b), the recovered samples exhibited reduced stress

and strain at break compared to the pristine state. The decline in mechanical strength can be mainly attributed to the limited number of dynamic structural units within the network and the relatively loose interconnection between crosslinked segments. The insufficient density of exchangeable bonds restricts effective stress redistribution, while weakened network connectivity diminishes load transfer efficiency, ultimately compromising the integrity of the crosslinked system (Xia *et al.* 2024). This reduced structural robustness is clearly evident in Figure 11(b), where both the control sample without NFC and the vitrimer containing only 3 wt.% NFC, despite being reprocessable, fractured during the early stages of the creep test and were unable to complete the measurement. This premature failure may be attributed to insufficient network consolidation after reprocessing, as networks with a high fraction of permanent crosslinks exhibit incomplete crosslink density recovery, leading to early fracture during creep deformation (Li *et al.* 2018).

In contrast, the composite containing 4 wt.% activated carbon and 4 wt.% NFC achieved nearly complete strain recovery (~100%), demonstrating a balanced viscoelastic response arising from the synergistic interaction between NFC reinforcement and activated carbon assisted stress distribution. NFC particles enhance stiffness and limit excessive chain slippage, while activated carbon promotes more uniform stress transfer without inducing excessive network mobility. Consequently, sufficient elastic restoring force is preserved to enable full recovery. For the same formulation subjected to reprocessing (Figure11(b)), the decrease in maximum creep strain while maintaining full recovery suggests enhanced network homogeneity and structural stabilization. As shown in Figure 11(a), the pristine composite with 5 wt.% NFC and 5 wt.% activated carbon showed the highest strain during the creep stage (1 to 5 min), indicating greater deformation under the applied load. This behaviour is consistent with the DMA results, where the same formulation showed the highest storage modulus, suggesting a highly stiff network capable of storing larger elastic deformation. However, the excessive activated carbon loading results in incomplete recovery with significant residual strain. This behaviour is attributed to excessive hard particles that generate stress concentration and interfacial inefficiencies, thereby diminishing creep resistance (cui *et al.* 2020). Consequently, the vitrimer contain 5 wt.% NFC and 5 wt.% formulation was unable to sustain the creep cycle after reprocessing. These results demonstrate that an appropriate filler ratio is critical for maintaining structural stability and achieving efficient viscoelastic recovery in vitrimer composites.

CONCLUSIONS

1. This study demonstrated the formation of a bio-based vitrimer network derived from epoxidised palm oil (EPO) through epoxy-anhydride and epoxy-acid curing with hexahydro-4-methylphthalic anhydride and citric acid. The resulting β-hydroxy ester linkages enabled thermally activated transesterification exchange, allowing dynamic rearrangement within the EPO-based vitrimer composite, while activated carbon and NFC provided additional physical reinforcement to the polymer matrix.
2. The formulation containing 5 wt.% NFC produced the highest storage modulus, demonstrating the strong reinforcing effect of NFC within the vitrimer network. The increased stiffness arises from the structural constraint imposed by the fibrous fillers, which restrict polymer chain mobility. However, this excessive network constraint

limited efficient bond exchange during creep-recovery and prevented effective reprocessing. The reduced swelling behaviour reflected the presence of a more compact and constrained polymer network, which contributed to the restricted molecular mobility.

3. The composite containing 4 wt.% activated carbon and 4 wt.% NFC exhibited the most balanced combination of stiffness, recovery behaviour, and reprocessability, achieving complete creep-recovery while maintaining sufficient network mobility. These results demonstrate that the mechanical performance and dynamic behaviour of short-backbone EPO vitrimer composite can be effectively tuned through filler composition, providing a promising strategy for developing sustainable and reprocessable palm oil-based polymer composites.

ACKNOWLEDGEMENTS

The authors gratefully acknowledge the financial support provided by the Ministry of Higher Education Malaysia (MOHE) through the Fundamental Research Grant Scheme (FRGS/1/2024/WAS03/UPM/02/4) under the Institute of Tropical Forestry and Forest Products. The authors also extend their sincere appreciation to the undergraduate students who assisted throughout the research.

Use of Generative AI

During the preparation of this work, the authors used the QuillBot Paraphrasing Tool solely to refine the language. After using the tool, the authors carefully reviewed and finalised all content, taking full responsibility for its accuracy and integrity.

REFERENCES CITED

Aigaje, E., Riofrio, A., and Baykara, H. (2023). "Processing, properties, modifications, and environmental impact of nanocellulose/biopolymer composites: A review," *Polymers* 15, article 1219. https://doi.org/10.3390/polym15061219

Akash, K., Parthasarathi, R., Kanmani Bharathi, J., and Elango, R. (2025). "Exploring the role of microbes in the biodegradation of plastic waste: Mechanisms, interactions, and implications for sustainable waste management-a review," *Water, Air, and Soil Pollution* 236(12), 1-49. https://doi.org/10.1007/s11270-025-08343-x

Aliyeva, F. K., Akhmedbekova, S. F., Isayev, N. Z., and Azizbeyli, E. I. (2023). "Study of the synthesis of vicinal dicarboxylic acid esters using the IR spectroscopy method," *Processes of Petrochemistry and Oil Refining* 24(3), 448-453.

Álvarez, M., Reilly, A., Suleyman, O., and Griffin, C. (2025). "A systematic review of epoxidation methods and mechanical properties of sustainable bio-based epoxy resins," *Polymers* 17, article 1956. https://doi.org/10.3390/polym17141956

Alwan Nassif, R., Hamid Hilal, R., and Khalid Khalef, W. (2024). "Enhancing anticorrosive characteristics of epoxy through nanocellulose reinforcement," *Iraqi Journal of Industrial Research* 11(3), 45-54. https://doi.org/10.53523/ijoirVol11I3ID391

Amin, O. (2026). "Revisiting properties of vitrimers: Special rheological and chemical

characteristics and reconsidered concepts," *Polymer Engineering & Science*. https://doi.org/10.1002/pen.70358

Anonymous. (2025). "Industry calls for Malaysia to maximise oil palm as biomass potential," *Bioenergy Insight*, Morden.

Aribam, B., Neihoikim, T., Horam, W., and Alam, W. (2025). "Removal of sulphate from drinking water sources using H_3PO_4 Chakhao rice husk activated carbon (CHAC): A comprehensive adsorption study," *Journal of Water Chemistry and Technology* 47(2), 167-180. https://doi.org/10.3103/S1063455X2502002X

Balakrishnan, P., Sreekala, M. S., Kunaver, M., Huskić, M., and Thomas, S. (2017). "Morphology, transport characteristics and viscoelastic polymer chain confinement in nanocomposites based on thermoplastic potato starch and cellulose nanofibers from pineapple leaf," *Carbohydrate Polymers* 169, 176-188. https://doi.org/10.1016/j.carbpol.2017.04.017

Beaumont, M., König, J., Opietnik, M., Potthast, A., and Rosenau, T. (2017). "Drying of a cellulose II gel: Effect of physical modification and redispersibility in water," *Cellulose* 24(3), 1199-1209. https://doi.org/10.1007/s10570-016-1166-9

Bertolo, M. R. V., Rodrigues, M. Á. V., Horn, M. M., Filho, J. G. de O., Marangon, C. A., Ferreira, M. D., and Ana Maria de Guzzi Plepis, and S. B. J. (2023). "Rheology of nanoscale polymer-based coatings," in: *Polymer-Based Nanoscale Materials for Surface Coatings* 2023, 131-149. https://doi.org/10.1016/B978-0-32-390778-1.00014-1

Bokobza, L. (2023). "Elastomer nanocomposites: Effect of filler-matrix and filler-filler interactions," *Polymer* 15, article 2900. https://doi.org/10.3390/polym15132900

Bonardd, S., Nandi, M., Hern, I., Maiti, B., Abramov, A., and David, D. (2023). "Self-healing polymeric soft actuators," *Chemical Reviews* 123, 736-810. https://doi.org/10.1021/acs.chemrev.2c00418

Cherik, D., and Louhab, K. (2017). "Preparation of microporous activated carbon from date stones by chemical activation using zinc chloride," *Energy Sources, Part A: Recovery, Utilization, and Environmental Effects* 39(18), 1935-1941. https://doi.org/10.1080/15567036.2017.1390012

Chin, K. L., Lee, C. L., H'ng, P. S., Rashid, U., Paridah, M. T., Khoo, P. S., and Maminski, M. (2020). "Refining micropore capacity of activated carbon derived from coconut shell via deashing post- treatment," *BioResources* 15(4), 7749-7769. https://doi.org/10.15376/biores.15.4.7749-7769

Chong, K. L., Lai, J. C., Rahman, R. A., Adrus, N., and Al-Saffar, Z. H. (2021). "Self-healable bio-based epoxy resin from epoxidized palm oil," *Chemical Engineering Transactions* 89, 379-384. https://doi.org/ 10.3303/CET2189064

Chu, Y., Sun, Y., Wu, W., and Xiao, H. (2020). "Dispersion properties of nanocellulose: A review," *Carbohydrate Polymers* 250, article 116892. https://doi.org/ 10.1016/j.carbpol.2020.116892

Collard, F., and Blin, J. (2014). "A review on pyrolysis of biomass constituents : Mechanisms and composition of the products obtained from the conversion of cellulose, hemicelluloses and lignin," *Renewable and Sustainable Energy Reviews* 38, 594-608. https://doi.org/10.1016/j.rser.2014.06.013

Cui, Y., Campbell, J. E., Burley, M., Patel, M., Hunt, K., and Clyne, T. W. (2020). "Effects of temperature and filler content on the creep behaviour of a polyurethane rubber," *Mechanics of Materials* 148, article 103461. https://doi.org/ 10.1016/j.mechmat.2020.103461

Dai, W., Yan, Q., Gao, J., Tan, X., Lv, L., Hou, H., Wei, Q., Yu, J., Wu, J., Yao, Y., Du, S., Sun, R., Jiang, N., Wang, Y., Kong, J., Wong, C., Maruyama, S., and Lin, C. (2019). "Metal-level thermally conductive yet soft graphene thermal interface materials," *ACS Nano* 13, 11561-11571. https://doi.org/ 10.1021/acsnano.9b05163

Dan, L., Xiaosheng, S., Yundong, M., and Yanhua, Z. (2014). "Two-dimensional Fourier transform infrared correlation spectroscopy studies on epoxy-phenol novolac network," in: *ECWC13 – 13th Electronic Circuits World Convention*, Nuremberg, Germany Two-Dimensional, 1-4. https://doi.org/10.1021/acsomega.1c02699

Denissen, W., Winne, J. M., and Du Prez, F. E. (2016). "Vitrimers: Permanent organic networks with glass-like fluidity," *Chemical Science* 7(1), 30-38. https://doi.org/10.1039/c5sc02223a

Dubey, P., Shrivastav, V., Maheshwari, P. H., and Sundriyal, S. (2020). "Recent advances in biomass derived activated carbon electrodes for hybrid electrochemical capacitor applications: Challenges and opportunities," *Carbon* 170, 1-29. https://doi.org/10.1016/j.carbon.2020.07.056

Fang, H., Ye, W., Ding, Y., and Winter, H. H. (2020). "Rheology of the critical transition state of an epoxy vitrimer," *Macromolecules* 53(12), 4855-4862. https://doi.org/10.1021/acs.macromol.0c00843

Feng, J., Wen, Y., Yang, W., Hu, X., Xu, Y., and Fang, Z. (2025). "Construction of an interpenetrating polymer network in situ to develop multifunctional cellulose nanofiber-enhanced films with superior mechanical performances," *International Journal of Biological Macromolecules* 304, article 140857. https://doi.org/10.1016/j.ijbiomac.2025.140857

Fuchs, J., Schuhmann, N., Alms, J., and Hopmann, C. (2026). "Advancing circular composite strategies by vitrimer-enabled reuse of unidirectional laminates," *Polymers* 18, article 300. https://doi.org/10.3390/polym18020300

Gan, P. G., Sam, S. T., Faiq, M., and Omar, M. F. (2020). "Thermal properties of nanocellulose-reinforced composites: A review," *Journal of Applied Polymer* 137(11), article 48544. https://doi.org/10.1002/app.48544

Ge, T., Pierce, F., Perahia, D., Grest, G. S., and Robbins, M. O. (2012). "Polymer welding: Strength through entanglements," *arXiv preprint arXiv*, 1211(6796), 1–5. https://doi.org/10.3390/polym18020300

Gheje, W. E., Abram, P. H., Tiwow, V. M. A., and Rahmawati, S. (2025). "Epoxidation of eugenol from clove oil (*Syzygium aromaticum*) using H_2O_2 oxidizer and H_3PO_4 catalyst," *Jurnal Akademia Kimia* 14(2), 77-82. https://doi.org/10.22487/j24775185.2025.v14.i2.pp77-82

Gong, L., Zhang, F., Peng, X., Scarpa, F., Huang, Z., Tao, G., Liu, H. Y., Zhou, H., and Zhou, H. (2022). "Improving the damping properties of carbon fiber reinforced polymer composites by interfacial sliding of oriented multilayer graphene oxide," *Composites Science and Technology* 224, article 109309. https://doi.org/10.1016/j.compscitech.2022.109309

Hu, F., Zeng, J., Cheng, Z., Wang, X., Wang, B., Zeng, Z., and Chen, K. (2021). "Cellulose nanofibrils (NFC) produced by different mechanical methods to improve mechanical properties of recycled paper," *Carbohydrate Polymers* 254, article 117474. https://doi.org/10.1016/j.carbpol.2020.117474

Jang, J. S., Varischetti, J., and Suhr, J. (2012). "Strain dependent energy dissipation in multi-scale carbon fiber composites containing carbon nanofibers," *Carbon* 50(11), 4277-4283. https://doi.org/10.1016/j.carbon.2012.05.012

Javier, F., and Toro, L. (2021). "Vitrimer-based bioinspired nanocomposites," Universität Freiburg.

Jawad, I. A. M., Al-hamdani, A. A., and Hasan, R. M. A. (2016). "Fourier transform infrared (FT-IR) spectroscopy of modified heat cured acrylic resin denture base material," *International Journal of Enhanced Research in Science, Technology & Engineering* 5(4), 130-140.

Jin, F., and Park, S. (2008). "Thermomechanical behavior of epoxy resins modified with epoxidized vegetable oils," *Polymer International* 57, 577-583. https://doi.org/10.1002/pi.2280

Jing, F., Zhao, R., Li, C., Xi, Z., Wang, Q., and Xie, H. (2022). "Influence of the epoxy/acid stoichiometry on the cure behavior and mechanical properties of epoxy vitrimers," *Molecules* 27, article 6335. https://doi.org/10.3390/molecules27196335

de Jong, E., Goumans, I., Visser, R., Puente, Á., and Gruter, G. J. (2025). "The opportunities and challenges of biobased packaging solutions," *Polymers* 17, article 2217. https://doi.org/10.3390/polym17162217

Jose, S. A., Cowan, N., Davidson, M., Godina, G., Smith, I., Xin, J., and Menezes, P. L. (2025). "A comprehensive review on cellulose nanofibers, nanomaterials, and composites: Manufacturing, properties, and applications," *Nanomaterials* 15, article 356. https://doi.org/10.3390/nano15050356

Karatrantos, A. V, Couture, O., Hesse, C., and Schmidt, D. F. (2024). "Molecular simulation of covalent adaptable networks and vitrimers: A review," *Polymers* 16, article 1373. https://doi.org/10.3390/polym16101373

Karoki, P. K., Kemefa, C. O., Kousika, R., Pu, Y., Cai, C. M., and Ragauskas, A. J. (2025). "Structure-performance relationships in lignin-based transesterification vitrimers: The role of lignin structural features," *Industrial Crops & Products* 237, article 122108. https://doi.org/10.1016/j.indcrop.2025.122108

Kelly, F. J., Wright, S. L., Woodward, G., and Fussell, J. C. (2025). "Plastic pollution and climate change: Double trouble," *Frontiers for Young Minds* 13, article 1719437. https://doi: 10.3389/fsci.2025.1636665

Khairkkar, S., Pansare, A. V., Pansare, S. V., Chhatre, S. Y., Sakamoto, J., Barbezat, M., Terrasi, G. P., Patil, V. R., Nagarkar, A. A., And, and Naito, M. (2025). "Adhesive-less bonding of incompatible thermosetting materials," *RSC Applied Polymers* 3(1), 247-256. https://doi.org/10.1039/d4lp00288a

Kotan, O., and Bayrakçeken, H. (2022). "Recycled human hair-derived activated carbon for energy-related applications," *Turkish Journal of Chemistry* 46, 184-192. https://doi.org/10.3906/kim-2105-70

Krishnan, B. P., Saalwaechter, K., Adjedje, V. K., And, and Binder, W. H. (2022). "Design, synthesis and characterization of vitrimers with low topology freezing transition temperature," *Polymers* 14(12), article 2456. https://doi.org/10.3390/polym14204338

Kumar, S. M., T., S., K., C., M., S., S., M. R., S., Siengchin, S., and Rajini, N. (2020). "Influence of fillers on the thermal and mechanical properties of biocomposites : An overview," in: *Biofiber and Biopolymers for Biocomposite*, 111-133. https://doi.org/10.32604/jrm.2022.017434

Lamm, M. E., Li, K., Ker, D., Zhao, X., Hinton, H. E., Copenhaver, K., Tekinalp, H., and Ozcan, S. (2022). "Exploiting chitosan to improve the interface of nanocellulose reinforced polymer composites," *Cellulose* 29(7), 3859-3870. https://doi.org/10.1007/s10570-021-04327-2

Lee, C. L., Bakar, B. F. A., Chin, K. L., Abdullah, L. C., Idris, N. I., and Chang, Q. R. (2025a). "Dual tuning effect of epoxy-to-curing agent ratio and PKS-based activated carbon loading on the mechanical and self-healing performance of epoxy vitrimer composites," *Polymer Engineering & Science*, 66(2), 1199-1219. https://doi.org/10.1002/pen.70270

Lee, C. L., Bakar, B. F. A., Chin, K. L., and Chuah, L. (2025b). "A review on the formulation and performance of EVO-based vitrimer: Stoichiometric calculations, curing agent functionalities and catalyst efficiency," *The Royal Society* 12, article 250612. https://doi.org/10.1002/pen.70270

Lee, C. L., H'ng, P. S., Chin, K. L., Paridah, M. T., Rashid, U., Maminski, M., Go, W. Z., Nazrin, R. A. R., Rosli, S. N. A., and Khoo, P. S. (2018). "Production of bioadsorbent from phosphoric acid pretreated palm kernel shell and coconut shell by two-stage continuous physical activation via N_2 and air," *Royal Society Open Science* 5(12), article 180775. https://doi.org/10.1098/rsos.180775

Li, L., Chen, X., Jin, K., Rusayyis, M. Bin, and Torkelson, J. M. (2021). "Arresting elevated-temperature creep and achieving full cross-link density recovery in reprocessable polymer networks and network composites via nitroxide-mediated dynamic chemistry," *Macromolecules* 54, 1452-1464. https://doi.org/10.1021/acs.macromol.0c01691

Li, L., Chen, X., Jin, K., and Torkelson, J. M. (2018). "Vitrimers designed both to strongly suppress creep and to recover original cross-link density after reprocessing: Quantitative theory and experiments," *Macromolecules* 51(15), 5537-5546. https://doi.org/10.1021/acs.macromol.8b00922

Li, Y., Wan, C., Li, H., Wang, F., Hu, F., and Cheng, Q. (2026). "A tung oil-based epoxy resin modifier enhances flexibility and superhydrophobicity," *Industrial Crops & Products* 240, article 122632. https://doi.org/10.1016/j.indcrop.2026.122632

Lou, L., Lopez, K. O., Nair, A. B., Desueza, W., and Agarwal, A. (2025). "Micro-mechanosensory insights from nature's mimosa leaves to shape memory adaptive robotics," *Materials and Design* 249, article 113567. https://doi.org/10.1016/j.matdes.2024.113567

Maisonneuve, L., Lebarbé, T., Grau, E., and Cramail, H. (2013). "Structure-properties relationship of fatty acid-based thermoplastics as synthetic polymer mimics," *Polymer Chemistry* 4(22), 5472-5517. https://doi.org/10.1039/c3py00791j

Malburet, S., Mauro, D., No, C., and Mija, A. (2020). "Sustainable access to fully biobased epoxidized vegetable oil thermoset materials prepared by thermal or UV-cationic processes," *RSC Advances* 10, 41954-41966. https://doi.org/10.1039/d0ra07682a

Masten-Davies, J., Quan, L., Tran, N., Zhang, J., and Varley, R. J. (2025). "Investigating the welding and healing of epoxy anhydride vitrimer carbon fibre composites," *Composites Part A* 196, article 108956. https://doi.org/10.1016/j.compositesa.2025.108956

Mauro, C. Di, Malburet, S., Genua, A., Graillot, A., and Mija, A. (2020). "Sustainable series of new epoxidized vegetable oil-based thermosets with chemical recycling properties," *Bio-Macromolecules* 21, 3923-3935. https://pubs.acs.org/doi/10.1021/acs.biomac.0c01059

Momin, A., Toda, M., and Wang, Z. (2025). "Investigation towards nanomechanical sensor array for real-time detection of complex gases," *Microsystems & Nanoengineering* 11, article 53. https://doi.org/10.1038/s41378-025-00899-2

Nakata, M. T., and Takahara, M. (2022). "Mechanics of reversible deformation during leaf movement and regulation of pulvinus development in legumes," *International Journal of Molecular Sciences* 23(18), article 10240. https://doi.org/10.3390/ijms231810240

Nuryanta, M. I., Aryaswara, L. G., Korsmik, R., Klimova-Korsmik, O., Nugraha, A. D., Darmanto, S., Kusni, M., and Muflikhun, M. A. (2023). "The interconnection of carbon active addition on mechanical properties of hybrid agel/glass fiber-reinforced green composite," *Polymers* 15, article 2411. https://doi.org/10.3390/polym15112411

Ogori, A. (2020). "Source, extraction and constituents of fats and oils," *HSOA Journal of Food Science & Nutrition* 2020(1), 1-22. https://doi.org/10.24966/FSN-1076/100060

Paramarta, A., and Webster, D. C. (2016). "Bio-based high performance epoxy-anhydride thermosets for structural composites: The effect of composition variables," *Reactive and Functional Polymers* 105, 140-149. https://doi.org/10.1016/j.reactfunctpolym.2016.06.008

Rajasekaran, S. J., and Raghavan, V. (2022). "Palmyra palm flower biomass-derived activated porous carbon and its application as a supercapacitor electrode," *Journal of Electrochemical Science and Engineering* 12(3), 545-556. https://doi.org/10.5599/jese.1314

Rana, S. S., and Gupta, M. K. (2021). "Fabrication of bionanocomposites reinforced with hemp nanocellulose and evaluation of their mechanical, thermal and dynamic mechanical properties," *Proceedings of the Institution of Mechanical Engineers, Part L: Journal of Materials: Design and Applications* 235(11), 2470-2481. https://doi.org/10.1177/14644207211004640

Ribeiro, D. C. M., Ramalho, A., Serra, A. C., and Coelho, J. (2025). "Biolubricants based on epoxidized vegetable oils: A review on chemical modifications, tribological properties, and sustainability," *Lubricants* 13, article 510. https://doi.org/10.3390/lubricants13120510

Roig, A., D'Agostino, V., Serra, À., and De la Flor, S. (2023). "Towards fast relaxation rates and creep resistance in disulfide vitrimer-like materials," *Reactive and Functional Polymers* 193, article 105764. https://doi.org/10.1016/j.reactfunctpolym.2023.105764

Sairi, N. N., Ibrahim, S., Hamzah, N., Ahmat, N., Hamza, M. F., Mohd, W., Wan, F., and Saleh, S. H. (2025). "Crosslinking effects on swelling, thermal and physicochemical properties of hemicellulose-based hydrogels," *Malaysian Journal of Chemistry* 27(5), 110-120. https://doi.org/10.55373/mjchem.v27n5.110

Salih, A. M., Ahmad, M. Bin, Ibrahim, N. A., HjMohd Dahlan, K. Z., Tajau, R., Mahmood, M. H., and Yunus, W. M. Z. W. (2015). "Synthesis of radiation curable palm oil-based epoxy acrylate: NMR and FTIR spectroscopic investigations," *Molecules* 20(8), 14191-14211. https://doi.org/10.3390/molecules200814191

Shaghaleh, H., Xu, X., and Wang, S. (2018). "Current progress in production of biopolymeric materials based on cellulose, cellulose nanofibers, and cellulose derivatives," *RSC Advances* 8, 825-842. https://doi.org/10.1039/c7ra11157f

Shi, Q., Jin, C., Chen, Z., An, L., and Wang, T. (2023). "On the welding of vitrimers: Chemistry, mechanics and applications," *Advanced Functional Materials* 33(36), article 2300288. https://doi.org/10.1002/adfm.202300288

Silva, D. F., César, J., Oliveira, R. De, and Aguiar, F. De. (2025). "Enzymatic synthesis of phenylethyl fatty esters from fixed oil extracted from *Syagrus coronata* (Mart.) Becc.," *Chemistry Proceedings* 18, article 17. https://doi.org/10.3390/ecsoc-29-26666

Sinaga, M. S., Tambun, R., Ndraha, E. E., and Ramadhan, A. Z. (2024). "The impact of hydrogen peroxide oxirane oxygen number conversion in epoxy compounds derived from purple passion fruit seeds," *Rasayan J. Chem* 17(1), 275-280. http://doi.org/10.31788/RJC.2024.1718733

Singh, G., Varshney, V., and Sundararaghavan, V. (2024). "Understanding creep in vitrimers: Insights from molecular dynamics simulations," *Polymer* 313, article 127667. https://doi.org/10.1016/j.polymer.2024.127667

Smith, M. K., and Northrop, B. H. (2014). "Vibrational properties of boroxine anhydride and boronate ester materials: Model systems for the diagnostic characterization of covalent organic frameworks," *Chemistry of Materials* 26, 3781-3795. https://doi.org/10.1021/cm5013679

Starr, F. W., Schrøder, T. B., and Glotzer, S. C. (2000). "Effects of a nano-sized filler on the structure and dynamics of a simulated polymer melt and the relationship to ultra-thin films," *Macromolecules* 35, 4481-4492. https://doi.org/10.1103/PhysRevE.64.021802

Stavila, E., Yuliati, F., Adharis, A., Laksmono, J. A., and Iqbal, M. (2023). "Recent advances in synthesis of polymers based on palm oil and its fatty acids," *RSC Advances* 13(22), 14747-14775. https://doi.org/10.1039/d3ra01913f

Su, C., Cheng, J., Zhang, J., and Gao, F. (2024). "Tertiary amine-based autocatalytic transesterification epoxy vitrimer: Effect of tertiary amine structure and covalent incorporation on the properties of vitrimers," *Polymer* 300, article 126958. https://doi.org/10.1016/j.polymer.2024.126958

Syduzzaman, M., Chowdhury, K. P., Fahmi, F. F., Rumi, S. S., and Hassan, A. (2024). "Effects of carbon-based nanofillers on mechanical, electrical, and thermal properties of bast fiber reinforced polymer composites," *Journal of Thermoplastic Composite Materials* 37(8), 2723-2774. https://doi.org/10.1177/089270572312167

Turku, I., Rohumaa, A., Tirri, T., and Pulkkinen, L. (2024). "Progress in achieving fire-retarding cellulose-derived nano/micromaterial-based thin films/coatings and aerogels: A review," *Fire* 7, article 31. https://doi.org/10.3390/fire7010031

Vanags, E., Kirpluks, M., Cabulis, U., and Walterova, Z. (2018). "Highly functional polyol synthesis from epoxidized tall oil fatty acids," *J. Renew. Mater*, 6(7), 764-771. https://doi.org/10.7569/JRM.2018.634111

Vardamides, J. C., Azebaze, A. G. B., Nkengfack, A. E., and Heerden, F. R. Van. (2006). "Scaphopetalone and scaphopetalumate, a lignan and a triterpene ester from *Scaphopetalum thonneri*," *Phytochemistry* 62(2003), 647-650. https://doi.org/10.1016/S0031-9422(02)00616-7

Vashchuk, A., and Kobzar, Y. (2022). "Chemical welding of polymer networks," *Materials Today Chemistry* 24, article 100803. https://doi.org/10.1016/j.mtchem.2022.100803

Wang, B., Hou, Y., Zhong, S., Zhu, J., and Guan, C. (2023). "Biomimetic Venus flytrap structures using smart composites: A review," *Materials* 16, article 6702. https://doi.org/10.3390/ma16206702

Wang, M., Miao, X., Li, H., and Chen, C. (2022). "Effect of length of cellulose nanofibers on mechanical reinforcement of polyvinyl alcohol," *Polymer* 14, article 128. https://doi.org/10.3390/polym14010128

Wang, T., Chen, H., Liang, W. J., Siang, B., Ng, L., Lu, R., Qi, J., Wang, H., Zhang, J., Xie, H., Xiao, R., and Huang, W. M. (2024). "Layered composites for high tan delta plateau over wide temperature range," *Polymers* 16, article 3587.

https://doi.org/10.3390/polym16243587
Wang, X., Zhang, L., Liu, Z., Zeng, Q., Jiang, G., and Yang, M. (2018). "Probing the surface structure of hydroxyapatite through its interaction with hydroxyl: A first-principles study," *RSC Advances* 8, 3716-3722. https://doi.org/10.1039/c7ra13121f
Wu, Y., Wei, Y., and Ji, Y. (2023). "Carbon material/vitrimer composites: Towards sustainable, functional, and high-performance crosslinked polymeric," *Giant* 13, article 100136. https://doi.org/10.1016/j.giant.2022.100136
WWF. (2022). "Circular economy for plastic in Malaysia – Are we on track," *malaysiakini*, https://www.malaysiakini.com/announcement/626174
Xia, J., Li, S., Gao, R., Zhang, Y., Wang, L., Ye, Y., Cao, C., and Xue, H. (2024). "Bio-based epoxy vitrimers with excellent properties of self-healing, recyclability, and welding," *Polymers* 16, article 2113. https://doi.org/10.3390/polym16152113
Xu, Z., Guo, Z., Xie, H., and Hu, Y. (2022). "Effect of Cd on pyrolysis velocity and deoxygenation characteristics of rice straw : Analogized with Cd-impregnated representative biomass components," *International Journal of Environmental and Public Health* 19, article 8953. https://doi.org/10.3390/ijerph19158953
Yan, W., Wang, Z., Luo, C., Xia, X., Liu, Z., Zhao, Y., Du, F., and Jin, X. (2022). "Opportunities and emerging challenges of the heterogeneous metal-based catalysts for vegetable oil epoxidation," *ACS Sustainable Chemistry and Engineering* 10, 7426-7446. https://doi.org/10.1021/acssuschemeng.2c00617
Yildirim, N., and Shaler, S. (2017). "A study on thermal and nanomechanical performance of cellulose nanomaterials (CNs)," *Materials* 10, article 718. https://doi.org/10.3390/ma10070718
Zhang, C., Cui, J., Sui, W., Gong, Y., Liu, H., Ao, Y., and Shang, L. (2023). "High heat Resistance , Strength , and toughness of epoxy resin with cellulose nanofibers and structurally designed ionic liquid," *Chemical Engineering Journal* 478, article 147063. https://doi.org/10.1016/j.cej.2023.147063
Zhang, L., Wang, R., Dai, Z., and Zhang, C. (2025). "Ion liquid selective depolymerization of epoxy resin insulation materials from electric power industry in a polar aprotic solvent system," *Reactive and Functional Polymers* 216, article 106456. https://doi.org/10.1016/j.reactfunctpolym.2025.106456
Zhang, S., Zheng, M., Tang, Y., Zang, R., Zhang, X., Huang, X., Chen, Y., Yamauchi, Y., Kaskel, S., and Pang, H. (2022). "Understanding synthesis–structure–performance correlations of nanoarchitectured activated carbons for electrochemical applications and carbon capture," *Advanced Functional Materials* 32, article 2204714. https://doi.org/10.1002/adfm.202204714

Article submitted: December 5, 2025; Peer review completed: January 9, 2026; Revised version received and accepted: March 19, 2026; Published: April 2, 2026.
DOI: 10.15376/biores.21.2.4457-4489